Rev. Adv. Mater. Sci. 44 (2016) 63-86

GALLIUM OXIDE: PROPERTIES AND APPLICATIONS – A REVIEW

S.I. Stepanov[1,2], V.I. Nikolaev[1,3], V.E. Bougrov[1] and A.E. Romanov[1,3]

[1]ITMO University, Kronverkskiy prospekt 49-A, St. Petersburg, 197101, Russia
[2]Peter the Great Saint-Petersburg Polytechnic University, Politekhnicheskaya str. 29, St. Petersburg, 195251, Russia
[3]Ioffe Physical-Technical Institute RAS, Politekhnicheskaya str. 26, St. Petersburg, 194021, Russia

Received: November 01, 2015

Abstract. Gallium oxide has attracted a considerable interest as a functional material for various applications. This review summarizes the research work carried out in the field of gallium oxide. Polymorphism, crystal structure, band-structure, optical and electrical properties are discussed. Various methods to produce Ga_2O_3 thin films, nanostructures and bulk crystals are covered. A special focus is given on potential applications of monoclinic polymorph β-Ga_2O_3. Finally, future perspectives of the research in the area of this material are discussed.

1. INTRODUCTION

Gallium oxide Ga_2O_3 belongs to a family of conducting transparent semiconducting oxides (TSO). Although gallium oxide has been known for decades it remained on the periphery of the mainstream research. The history of gallium oxide dates back to 1875 when Lecoq de Boisbaudran [1] described newly discovered element gallium and its compounds. The early publications focused on the basic research of the material as such. Later on new applications were developed and Ga_2O_3 was investigated from the standpoints of microwave and optical maser studies, as a material for phosphors and electroluminescent devices, for chemical sensing and catalysis, as transparent conductive coatings etc. Gallium oxide scientific and technological research has greatly intensified over the last decade as the potential of Ga_2O_3 as the perspective wide band gap semiconductor has been recognized. Purity and crystalline quality have never been a primary concern in the conventional applications of gallium oxide. On the other hand, semiconductor applications set much higher standards for the material quality and purity similar to those accepted for established semiconductors like Si or GaAs. This was a turning point in the development of Ga_2O_3 research as new approaches not only opened perspectives for Ga_2O_3 in semiconductor applications, but also boosted the research field as a whole.

2. PHYSICAL PROPERTIES

2.1. Polymorphism

Gallium oxide can form several different polymorphs, designated as α-, β-, γ-, δ-, ε [2]. A transient κ-Ga_2O_3 polymorph has been also reported [3] (see Table 1). Polymorphs are different not only in their crystal space group but also in the coordination number of Ga ions. All of these phases of gallium oxide can be prepared under specific conditions [2,4]. The first polymorph, α-Ga_2O_3 is rhombohedral, space group $R\bar{3}c$, analogous to corundum (α-Al_2O_3). This polymorph can be synthesized by heating GaO(OH) in air between 450 °C and 550 °C [2]. The second form, β-Ga_2O_3 has monoclinic structure and belongs to space group C2/m. This form of Ga_2O_3 can be obtained by baking any other polymorph of Ga_2O_3 in air at sufficiently high tempera-

Corresponding author: A.E. Romanov, e-mail: alexey.romanov@niuitmo.ru

Table 1. Ga_2O_3 polymorphs.

Polymorph	Structure	Space group	Lattice parameters	Comment	Reference
a	rhombohedral	$R\bar{3}c$	a = 4.9825 Å c = 13.433 Å	Experimental	Marezio [136]
			a = 5.059 Å c = 13.618 Å	Calculated	Yoshioka [5]
			a = 5.04 Å c = 13.56 Å	Calculated	He [17]
b	monoclinic	C2/m.	a = 12.23 Å b = 3.04 Å c = 5.80 Å β = 103.7°	Experimental	Kohn [8]
			a = 12.27 Å b = 3.04 Å c = 5.80 Å β = 103.7°	Calculated	He [137]
			a = 12.214(3) Å b = 3.0371(9) Å c = 5.7981(9) Å β = 103.83(2)°	Experimental	Ahman [12]
g	cubic	$Fd\bar{3}m$	a = 8.238 Å	Experimental	Zinkevich [138]
			a = 8.30±0.005 Å	Experimental	Arean [96]
d	body-centred cubic	$Ia\bar{3}$	a = 10.00 Å	Experimental	Roy [2]
			a = 9.401 Å	Calculated	Yoshioka [5]
	“δ-Ga_2O_3” is a form of ε-Ga_2O_3 and not a distinct polymorph				Playford [3]
e	orthorhombic	$Pna2_1$	a = 5.120 Å b = 8.792 Å c = 9.410 Å	Calculated	Yoshioka [5]

ture. As it comes to other polymorphs, little data is available because structural characterisation has been hampered by their typically poorly crystalline nature. It is commonly agreed that the third form, γ-Ga_2O_3 has defective cubic spinel-type structure ($MgAl_2O_4$-type) with $Fd\bar{3}m$ space group. The fourth and fifth polymorphs, called δ-Ga_2O_3 and ε-Ga_2O_3 were first synthesized and described by Roy et al. [2] in 1952. The authors proposed that δ-Ga_2O_3 form has a C-type rare-earth structure analogous to Mn_2O_3 and In_2O_3. As for ε-Ga_2O_3 polymorph, Roy et al. were able to measure powder X-ray diffraction pattern which was distinct from all other known polymorphs, but could not determine the structure of the ε polymorph. A more recent publication by Playford et al. [3] shows that the original assumption was not correct as “δ-Ga_2O_3” is merely a nanocrystalline form of ε-Ga_2O_3 and not a distinct polymorph. The structure of ε-Ga_2O_3 was simulated using density functional theory, in the space group $Pna2_1$, the same as for κ-Al_2O_3 and ε-Fe_2O_3 by Yoshioka [5]. On the contrary, experimental results presented by Playford et al. do not support that assumption as ε-Ga_2O_3 was found to belong to $P6_3mc$ group of symmetry. The structure is similar to that of a disordered hexagonal ε-Fe_2O_3 [6]. Playford et al. also observed the formation of a transient polymorph κ-Ga_2O_3 which is an analogue of orthorhombic κ-Al_2O_3.

2.2. Properties of β-Ga_2O_3

The β-form is the most common and the well-studied polymorph of gallium oxide. β-Ga_2O_3 is the only stable polymorph through the whole temperature range till the melting point, whilst all other polymorphs are metastable and transform into the β-Ga_2O_3 at temperatures above 750-900 °C [7]. Thermal stability of β-Ga_2O_3 makes it possible to produce bulk single crystals and epitaxial films via high temperature processes such as crystallisation from a melt or vapour phase epitaxy. Among other polymorphs of gallium oxide, β-Ga_2O_3 has attracted more attention from the researches because of its avail-

Table 2. Physical properties of β-Ga_2O_3

Property	Value	Reference
Crystal structure	Monoclinic	[9,12]
Group of symmetry	C2/m	[9,12]
Lattice parameters		
a	12.214(3) Å	[12]
b	3.0371(9) Å	[12]
c	5.7981(9) Å	[12]
β	103.83(2)°	[12]
Density	5.95 g/cm^3	[85,87,139]
Dielectric constant	9.9-10.2	[28]
	13.9	[140]
Band gap	4.85±0.1 eV	[22]
Melting point	1795 °C	[88]
	1795±15 °C	[141]
	1740 °C	[2]
	1820±20 °C	[23]
Specific heat	0.56 Jg^{-1}K^{-1}	[14]
	0.49 Jg^{-1}K^{-1}	[85]
Thermal conductivity		
[100]	10.9±1.0 W/mK	[15]
	13 W/mK	[13]
[-201]	13.3±1.0 W/mK	[15]
[001]	14.7±1.5 W/mK	[15]
[110]	27.0±2.0 W/mK	[15]
	21 W/mK	[14]
Refractive index @532nm		
|| [010]	1.9523	[29]
⊥(100)	1.9201	[29]

ability and outstanding properties. Although β-Ga_2O_3 is well characterized compared to other Ga_2O_3 polymorphs, there are still some discrepancies in published data on material properties.

2.3. Crystal structure

The lattice parameters of β polymorph of gallium oxide were reported first by Kohn et al. [8], and the structure was determined by Geller [9] in space group C2/m. Negative tests for piezo- and pyroelectricity supported the conclusion that the most probable space group for the crystal was C2/m. Walton and Chase [10] pointed out that the morphological symmetry of the crystals appeared to be lower than that of the accepted point group 2/m. Optical and SEM studies also supported the assignment of the lower symmetry to β-Ga_2O_3. They suggested that the crystal cell of β-Ga_2O_3 is of the pseudosymmetrical triclinic structure and the true space group should be P1. However, this conclusion was questioned by other scientists working in the field. As pointed out by Geller [11], there had been numerous other investigations on crystals β-Ga_2O_3 and none of these had indicated deviation from the monoclinic structure. Therefore, the deviation, if any, from the more symmetric structure must be very small, indeed.

The most recent and accurate study of β-Ga_2O_3 crystal structure was published by Ahman et al. [12]. Even though the results show a rather small difference with the previously published data of Konh [8] and Geller [9], the precision of that study was about ten times better than in the previous works. The X-ray diffraction symmetry and systematic extinctions clearly indicated a C-centred monoclinic cell with space group C2/m. Refinement of the structure in space group P1 gave no further improvement. The unit cell of β-Ga_2O_3 is shown in Fig. 1. It contains two crystallographically inequivalent Ga positions, one with tetrahedral geometry Ga (I) and one with octahedral geometry Ga (II). The oxygen ions are arranged in a “distorted cubic” close-packed array. Oxygen atoms have three crystallographically different positions and are denoted as O(I), O(II) and O(III), respectively. Two oxygen atoms are coordinated trigonally and one is coordinated tetrahedrally.

2.4. Thermal properties

Compared to other semiconductors, β-Ga_2O_3 is a poor thermal conductor. Its thermal conductivity is about half of that of sapphire and one order of magnitude smaller than that of GaN. Because of the crystalline anisotropy, the thermal conductivity in β-Ga_2O_3 is very different along different crystal directions. The thermal conductivity is the highest along the [010] direction, and lowest along the [100] direction at all temperatures used in the measurements. Thermal conductivity measured by laser-flash methods is 13 W/mK along the [100] direction [13] and 21 W/mK along the [010] direction [14]. Guo et al. measured the temperature-dependent thermal conductivity along four different crystal directions in the temperature range of 80-495K using the time domain thermoreflectance method. At room temperature, the [010] direction has the highest thermal conductivity of 27.0±2.0 W/mK, while that along the [100] direction has the lowest value of 10.9±1.0 W/mK [15].

The thermal conductivity can be fitted to a formula $k(T) = AT^{-m}$, where the exponent m is around 3.5 for low temperature range (80-200K) and 1.2 for high temperature range (200-495K) [15]. At low temperatures, the thermal conductivity of β-Ga_2O_3 does

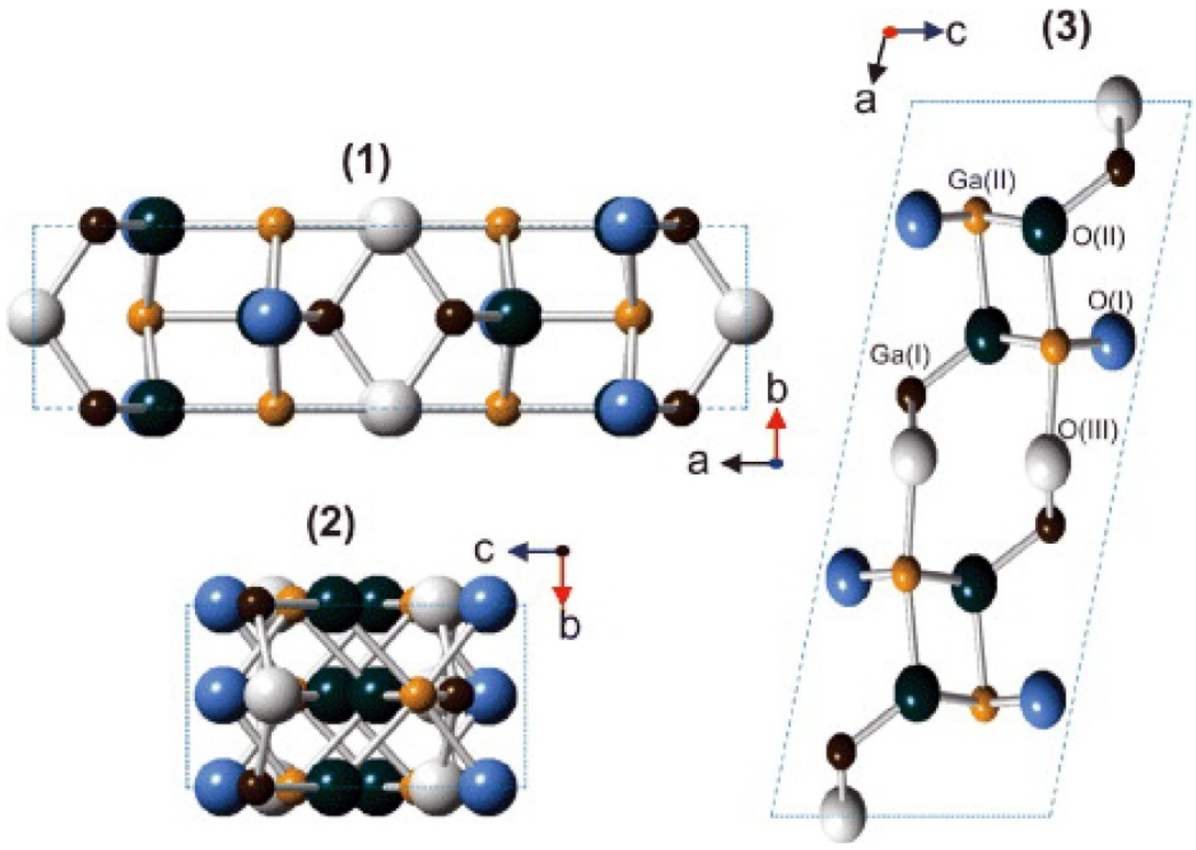

Fig. 1. Unit cell of β-Ga_2O_3. It possesses two inequivalent Ga sites: Ga(I), Ga(II) and three inequivalent O-sites: O(I), O(II) and O(III). Depicted is the projection of the unit cell of β-Ga_2O_3 along the c-(1), a-(2) and b-axis (3). Reprinted with permissions from C. Janowitz, V. Scherer, M. Mohamed, A. Krapf, H. Dwelk, R. Manzke, Z. Galazka, R. Uecker, K. Irmscher and R. Fornari // *New J. Phys.* **13** (2011) 085014, © 2011 IOP Science.

not exhibit the typical $T^{-3/2}$ dependence on temperature, indicating that heat conduction is limited not only by phonon scattering but also by free electron scattering [14,15].

2.5. Electronic structure

Up to now, several theoretical studies on the electronic structure of the β-Ga_2O_3 have been published [5,16-20]. Density functional theory (DFT) approach was used in works [16,19]. Although DFT modelling can provide satisfactory qualitative description for the electronic structure, it tends to underestimate band gap values. This is because DFT is based on the ground state theory, which results in the underestimated exchange-correlation potential among the excited electrons [19]. More accurate results were obtained using hybrid density functional theory [17,20,21]. Hybrid functional allows to produce more accurate results for structure and energetics, and band gaps in much better agreement with experiment.

All studies arrived at a similar conclusion that the conduction-band minimum in β-Ga_2O_3 was located at the Γ point and the valence band was almost flat. However the authors disagreed on the position of the valence band maximum. Though, due to the small dispersion of the valence band, its exact location does not substantially affect the magnitude of the band gap. According to He et al. [17] the valence band maximum appears to be almost degenerate at the Γ and M k-points for β-Ga_2O_3; the energy at Γ being 0.03 eV lower than that at M. On the other hand, the conduction band minimum occurs at Γ, so there is a direct gap of 4.69 eV at Γ and an indirect M-Γ gap of 4.66 eV. On the contrary, Varley et al. [21] found that the valence band maximum is located just off of the M point. This results in the indirect band gap of 4.83 eV, which is slightly smaller than the direct band gap of 4.87 eV at Γ. Peelaers et al. [20] also concluded that the fundamental band gap of β-Ga_2O_3 is indirect and has a magnitude of 4.84 eV. The valence band maximum is located on the I–L line, which is on the face of the Brillouin zone. The direct band gap at Γ is only 0.04 eV larger (4.88 eV). Analysis of the dipole matrix elements reveals that while the vertical transitions are dipole-allowed at the Γ point and at the VBM, they are roughly an order of magnitude weaker at the VBM and rapidly decrease to 0 at the M-point. The weakness of the indirect transitions and the small energy difference between indirect and direct gaps effectively make β-Ga_2O_3 a direct-gap material, consistent with the experimentally observed sharp absorption onset at ~4.9 eV [21].

According to calculations, the electron effective mass is small and almost isotropic. Values between 0.27 and 0.28 m_e, depending on the direction were reported by Peelaers et al. [20]. Similar values of 0.281±0.005 m_e [21] and 0.276 m_e [17] were reported by other researchers. These results agree very well with experimental measurements (0.28 m_e) [22]. The valence band is almost flat indicating a rather large effective mass for holes. The effective hole mass along the Γ-Z direction was estimated to

be around 40 m_e, also much smaller m^*_h of 0.40m_e was found along the Γ-A direction [21].

Experimental research of the β-Ga_2O_3 electronic structure was performed by Janowitz and co-workers [22]. The authors employed angular resolved photoemission (ARPES) for the determination of the fundamental gaps and band structure along high-symmetry directions. A detailed comparison of bands determined by ARPES along major high-symmetry lines showed nearly perfect agreement with the theory. Also the effective masses of Ga_2O_3 showed good agreement with the theory. The indirect band gap of 4.85±0.1 eV has been reported.

2.6. Optical properties

Owing to its wide band gap, pure stoichiometric β-Ga_2O_3 is colourless and highly transparent up to UV-C range of the light spectrum. However, colouration of the crystals can be caused by impurities or specific growth conditions. A strong correlation between conductivity and optical properties has been reported by Galazka et al. [14,23]. Insulating β-Ga_2O_3 crystals were either colourless or had a light yellowish colouration which was caused by some minor absorption in the blue part of the visible spectrum. Conductive n-type crystals had bluish colouration which was caused by increased free carrier absorption in the red and NIR regions of the spectrum. The red and NIR absorption has been assigned to plasma absorption by conduction electrons. Greyish colouration is caused by impurities e.g. carbon. Quantitatively, this can be seen in Fig. 2 which shows optical transmittance spectra for Ga_2O_3 crystals with different concentration of free electrons [14]. For the samples with low electron concentration the transmittance spectra showed a steep absorption edge at 255-260 nm and virtually full transparency to the NIR wavelength range. The transmittance in the visible and NIR wavelengths deteriorates with increasing free electron concentration.

The absorption spectra typically exhibits a short cut off absorption edge at around 255-260 nm with a shoulder around 270 nm. The absorption at 255-260 nm can be attributed to the transition from the valence band to the conduction band [24]. As found by Ueda et al. [25], absorption is sensitive to the polarization of the incident light. The fundamental absorption edges for E||b and E||c are 253 nm and 270 nm, respectively. These transitions are interpreted as the direct-allowed ones from the valence band with Γ_2^- symmetry to the bottom of the conduction band with Γ_1^- and from Γ_1^- to Γ_1^+ respectively. Villora et al. [26] questioned this model as it failed to explain the observed discrepancy between absorption and excitation spectra. Instead it was suggested that the 270 nm absorption band was due to the transition from the valence band perturbed by Ga^{3+} vacancies to the conduction band, while the band with the edge at 260 nm was due to the intrinsic band-to-band transition.

Refractive index of β-Ga_2O_3 was calculated theoretically from the first principles [17], measured experimentally for thin films [27,28] and bulk single crystals [29]. Bhaumik and co-workes [29] measured temperature-dependent refractive index along

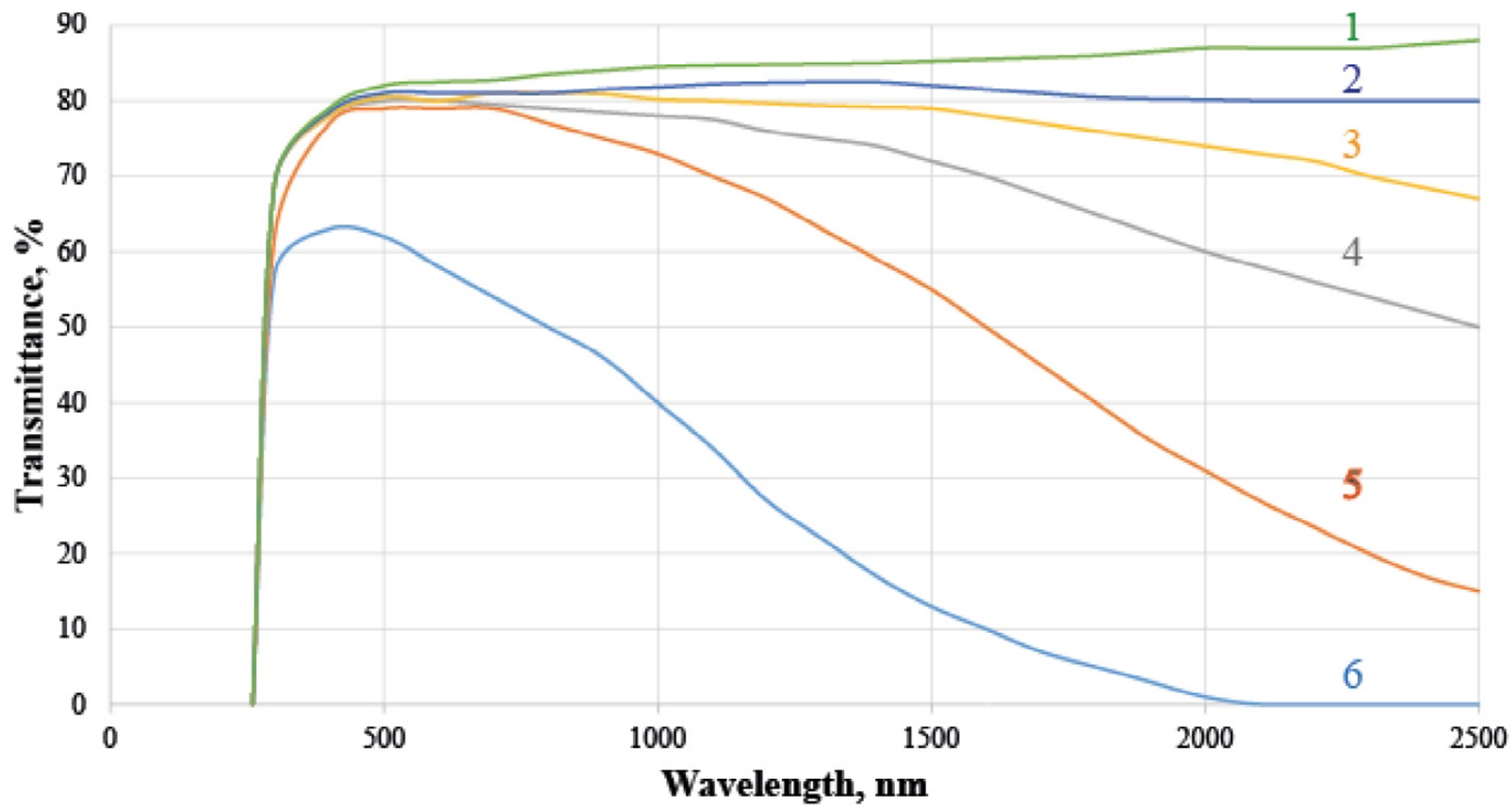

Fig. 2. Transmittance spectra of as-grown β-Ga_2O_3 single crystals obtained by the Czochralski method with various free electron concentrations: 1 – insulating (doped with Mg); 2 - 4·10^{16} cm^{-3}, 3-3.5·10^{17} cm^{-3}; 4-5.2·10^{17} cm^{-3}; 5-2.2·10^{18} cm^{-3}; 6-1·10^{19} cm^{-3} (Sn). Wafer orientation was (100) and thickness about 0.5 mm. According to data from Ref. [14].

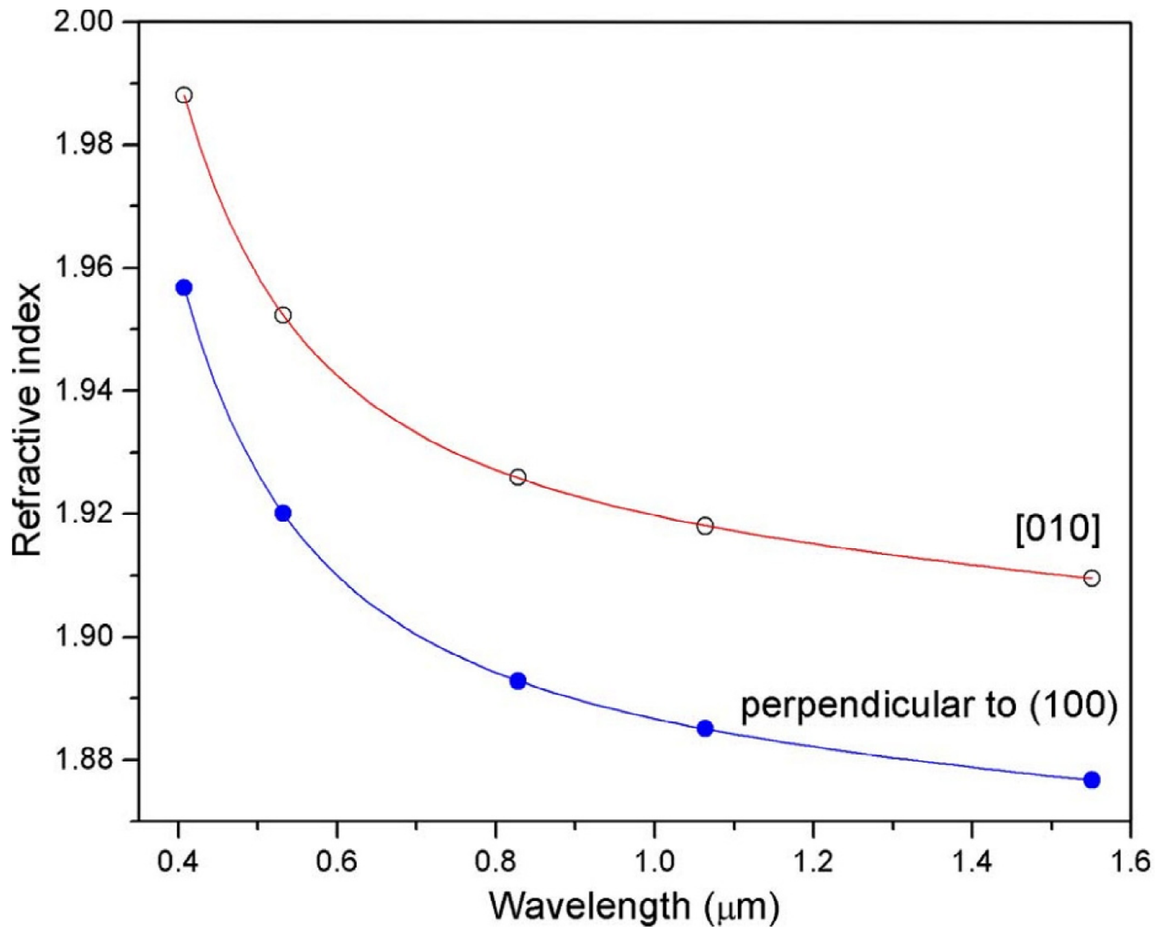

Fig. 3. Room temperature refractive index of β-Ga_2O_3. Reprinted with permissions from I. Bhaumik, R. Bhatt, S. Ganesamoorthy, A. Saxena, A. K. Karnal, P.K. Gupta, A. K.Sinha and S.K. Deb // *Appl. Opt.* **50** (2011) 6006, © 2011 OSA Publishing.

the [010] crystallographic direction and the direction perpendicular to (100)-plane for β-Ga_2O_3 single crystals grown by the floating zone technique (see Fig. 3). Also, they formulated Sellmeier equation coefficients for wavelengths in the range of 0.4–1.55 μm at different temperatures in the range of 30–175 °C. It was found that the refractive increases linearly with temperature and the thermal coefficient of refractive index at about 10^{-5}/°C).

The β-Ga_2O_3 can exhibit up to three different emissions, UV (3.2-3.6 eV), blue (2.8-3.0 eV), and green (2.4 eV) bands [30-32]. The UV band emission is independent of the sample preparation method and impurities. Bearing in mind that the β-Ga_2O_3 band gap is 4.8 eV, it seems highly unlikely that UV luminescence originates from band-edge recombination. Instead, UV band can be attributed to the recombination of free electrons and a self-trapped holes [33]. There is a correlation between the blue band intensity and resistivity in β-Ga_2O_3 crystals [34]. This indicates that oxygen vacancies, presumably responsible for the n-type conductivity, are also involved in the blue emission process. Harwig and Kellendonk [32] suggested that the blue emission originates from the recombination of an electron on a donor and a hole on an acceptor. Possible donors are V_O and Ga_i, and possible acceptors are V_{Ga} and/or the V_O-V_{Ga} complex [32]. The green emission was obtained only after doping the samples with specific elements. The most efficient green emission was obtained by the introduction of Be, Ge, Sn, and to a lesser extent, Li. Fe and Cu both acted as a killer for the blue emission [32]. The green luminescence was proposed to be associated with self-trapped or bound excitons by Villora et al. [26].

2.7. Growth and deposition methods

Gallium oxide crystals films and nanostructures can be synthesized by a variety of techniques, including sputtering [35-37], laser ablation [38,39], sol–gel [36,40], chemical vapour deposition [41-43], etc. Bulk crystals can be synthesized by melt growth techniques. Poly- and singlecrystalline films of Ga_2O_3 can be deposited on native (Ga_2O_3) and foreign (Al_2O_3, Si, GaAs, TiO_2, $BaTiO_3$, MgO, etc) by various methods.

2.7.1. Chemical synthesis

Polycrystalline and nanocrystalline Ga_2O_3 can be synthesized using a number of simple chemical routes. The advantages of solution deposition route include simple equipment, low temperature deposition, large area coverage and high throughput. In publication [44] Ga_2O_3 films on $BaTiO_3$ substrates were produced by spraying aqueous solution of $Ga(NO_3)_2$. The spray was developed by an ultrasonic nebuliser and was directed towards the substrate by a carrier gas of humid air. The deposition temperature was 300 °C. After deposition, the film was annealed in air or flowing oxygen. Ga_2O_3 films were produced by a spray pyrolysis process [45]. A solution of $GaCl_3$ in ethanol was sprayed over a hot (700-

800 °C) quartz and thermally oxidized silicon substrates. The deposition was carried out in air. The film was determined to be a polycrystalline β-Ga_2O_3 with mean grain size of 80 nm. Deposition rate as high as 8 nm/s was achieved.

Highly crystalline α-phase Ga_2O_3 thin films were grown on *c*-sapphire substrates by mist chemical vapour deposition at 400 °C [43]. Gallium acetylacetonate $Ga(C_5H_7O2)_3$ in a solvent mixture of distilled water, hydrochloric acid (HCl), and peroxide (H_2O_2) were used as precursors. Gallium acethylacetonate $Ga(C_5H_7O2)_3$ is a relatively low-cost, easy to handle material and is widely used as a source material for the Ga_2O_3 synthesis. In publication [46] $BaTiO_3$ substrates were dipped in a methanol solution of gallium acetylacetonate and then baked in a furnace for 30 s at 600-950 °C. This first heat treatment resulted in amorphous Ga_2O_3 films. After second heat treatment at 1020 °C in an Ar gas atmosphere the films turned into β-Ga_2O_3.

A modification of this method employing a sol-gel approach was reported by the same research group [46,47]. In this case, H_2O and HCl were added into the acethylacetonate solution in methanol and mixed at 50 °C for 1-5 h to promote a sol-gel transition. $BaTiO_3$ ceramic substrates were immersed in the solution. The solution-coated ceramic sheets were then dried for about 5 min in air at RT before being heated in a furnace for 10 min in air in the range 600 - 1000 °C. In contrast to the deposition process using a methanol solution of gallium acetylacetonate, no rapid heating was needed. Therefore, the sol-gel process is more suitable for large-area coatings.

2.7.2. Thermal vaporization and sublimation

This group of methods relies on the fact that Ga_2O_3 decomposes into volatile lower oxides and oxygen at elevated temperatures. At lower temperatures the reaction reverses to produce Ga_2O_3 crystals. Since the underlying mechanism involves chemical transformations, these methods should be classified as chemically assisted vapour transport. However, they are often referred as physical vapour transport or sublimation growth. Maslov et al. [48] studied sublimation growth of Ga_2O_3 films on sapphire substrates of different orientations. Gallium (III) oxide powder was heated in sapphire crucible covered with sapphire substrate. The deposition was carried out at the temperature of 1350 °C under argon ambient. Growth on *a*-, *c*- and *r*-sapphire resulted in predominantly (111) polycrystalline films. In contrast, growth on *m*-plane sapphire resulted in amorphous-like material. The best results were achieved for *a*-plane sapphire substrates where the fastest growth rate and the best degree of orientation were achieved. Butt et al. [49] described chemical vapour transport of gallium oxide in reducing atmosphere containing hydrogen. The addition of hydrogen facilitates the formation of volatile oxides. As it was shown by the authors, Ga_2O_3 vaporises in H_2 as Ga_2O(g) at elevated temperatures. The Ga_2O(g) moves to cooler zones of the furnace, back reacts with H_2(g) and H_2O(g) and condenses out as Ga(l) and Ga_2O_3(s). Penner et al. [50] reported on the deposition of Ga_2O_3 films by thermal evaporation under vacuum. Gallium (III) oxide powder was thermally evaporated from a tantalum crucible onto vacuum- cleaved NaCl (001) surfaces at varying substrate temperatures (298K–580K), deposition rates (<~0.3–10 Å s^{-1}) and O_2 background pressures (up to 10^{-2} Pa O_2). The morphology of the Ga-oxide films was found to be mainly determined by the interaction of substrate temperature, deposition rate and rate of re-oxidation. The films turned out to be almost amorphous at any temperature below 773K. Crystalline β-Ga_2O_3 structures were both obtained after oxidative and reductive treatments at and beyond 773K.

2.7.3. Chemical vapour deposition

In a chemical vapour deposition (CVD) process Ga_2O_3 is produced by a chemical reaction of vapour-phase precursors on a heated substrate. A wide range of Ga compounds has been employed for the synthesis of Ga_2O_3 by CVD techniques. Gallium trichloride $GaCl_3$ [51] and monochloride GaCl [41,52] were used as precursors for Ga_2O_3 deposition. $GaCl_3$ can be vaporised at moderate temperatures (around 150 °C). While $GaCl_3$ is stable at normal condition, the monochloride form exists only at temperatures above 600 °C. Therefore, GaCl is synthesized upstream the reactor by passing hot HCl gas over Ga metal. The produced GaCl vapour is transported to the deposition zone of the reactor in a stream of a carrier gas where it reacts with an oxidizing agent to produce Ga_2O_3. This method is also often referred to in literature as halide vapour phase epitaxy (HVPE).

Metal-organic chemical vapour deposition (MOCVD) of Ga_2O_3 using precursors such as trimethylgallium ($Ga(CH_3)_3$, TMG) and triethylgallium ($Ga(C_2H_5)_3$, TEG), has been extensively studied for the deposition of Ga_2O_3 thin films. Oxidizing agents, like oxygen, nitrous oxide (N_2O) and water, have been utilized to ensure the deposition of high qual-

ity thin films. Mi et al. [53] used trimethylgallium and oxygen precursors and nitrogen was used as the carrier gas. The growth pressure was kept at 20 Torr and the substrate temperature was 600-700 °C. The XRD analyses showed that the films deposited at 650 °C were pure β-Ga_2O_3. Ravadgar et al. [54] reported on MOCVD-grown single-crystal β-Ga_2O_3 epilayers on (0001) sapphire. The epilayers were grown using a commercial Emcore D180 MOCVD system. TMG and pure oxygen (99.999%) were employed as precursors. Pure Ar (99.999%) was used as the carrier gas. Epilayers were grown at low pressure of 15 Torr at a relatively low temperature of 450 °C. As-grown epilayers were annealed at 700 °C and 800 °C for 30 min in atmosphere. Highly [$\bar{2}$01] oriented single-crystal β-Ga_2O_3 epilayers were produced. It was found, that annealing in atmosphere at 700 °C and 800 °C can heal their surface states and point defects without disturbing the average crystalline structure and quality. Gogova et al. [55] studied low-pressure MOCVD growth of Ga_2O_3 films on sapphire and native Ga_2O_3 substrates. In contrast to the other reports, water vapour was used as the oxygen source. Trimethylgallium and argon were used as a source of gallium and a carrier gas, respectively. The reactor pressure was set at 10-15 mbar. The deposition temperature of 800 °C was selected. The produced films were oriented β-Ga_2O_3 and exhibited an epitaxial relationship with the hexagonal substrate. A comparative study of oxygen and water precursors for the MOCVD growth of Ga_2O_3 has been conducted by Wagner and co-workers [56]. Growth using oxygen as oxidant resulted in nano-crystals in form of wires or agglomerates. In contrast, with water as an oxidant, smooth homoepitaxial β-Ga_2O_3 layers were obtained under optimized conditions.

Unlike CVD where the reacting gases are continuously supplied to the reactor, atomic layer deposition (ALD) utilizes iterative, self-saturating precursor exposures to reacting gases which are delivered separately to react with the surface instead of with each other. Each reaction is self-limiting and a single layer is deposited at each cycle. As a result, ALD enables precise thickness control and excellent uniformity. Comstock and Elam [57] demonstrated ALD growth of Ga_2O_3 thin film using TMG as a source of Ga. The authors evaluated a variety of oxygen precursors including H_2O, H_2O_2, isopropanol, O_2, O_3, and H_2O/O_2, but found that only ozone was effective. The Ga_2O_3 growth was self-limiting with a growth rate of <~0.52 Å/cycle between 200 and 375 °C. Moreover, the Ga_2O_3 films were stoichiometric, free of residual carbon, and exhibited properties similar to those for bulk Ga_2O_3. Scanning electron microscopy revealed smooth films with good step coverage over trench structures, and X-ray diffraction showed that the films were amorphous as-deposited but crystallized to β-Ga_2O_3 upon annealing at 900 °C.

Many other less common compounds have been used as precursors for the CVD growth of Ga_2O_3. Kim et al. [58] produced amorphous Ga_2O_3 on Si(100) substrates using gallium isopropoxide as single precursor without any extra oxygen source or carrier gas. Battiston et al. [42] deposited Ga_2O_3 thin films using gallium tris-hexafluoroaeetylacetonate ($Ga(hfae)_3$) and oxygen precursors. Mîinea et al. [59] described low pressure CVD synthesis of Ga_2O_3 from $Ga[OCH(CF_3)_2]_3HNMe_2$ and air at 250–450 °C. Nieminen et al. [60] studied ALD deposition of Ga_2O_3 films using gallium acethylacetonate $Ga(C_5H_7O_2)_3$ and water, oxygen or ozone as precursors. Basharat et al. [61] reported on aerosol assisted CVD of Ga_2O_3 using diethylalkoxogallanes precursors. The precursors were synthesized in situ by reaction of TEG and ROH ($R=CH_2CH_2NMe_2$, $CH(CH_3)CH_2NMe_2$, $C(CH_3)_2CH_2OMe$, $CH(CH_2NMe_2)_2$) in toluene.

2.7.4. Molecular beam epitaxy

Molecular Beam Epitaxy (MBE) growth of Ga_2O_3 has been reported in [62-67]. Conventional Knudsen cells were used to supply Ga and dopant (Si, Sn) fluxes. Pure oxygen was found to be inefficient since almost all of the supplied oxygen molecules re-evaporated [64]. For that reason either RF plasma [63,66,67] or ozone [62,64,65] sources were used instead. The ozone MBE system has the advantage of higher growth rates up to 0.7 μm/hr [65]. In contrast, the highest growth rate reported for the Ga_2O_3 deposition by plasma MBE is only 132 nm/hr [67]. However, the precise control of the intentional doping densities in Ga_2O_3 (010) films grown by an ozone MBE is difficult because of the high background pressure (>10^{-4} Torr) [67]. Sasaki et al. [65] found that the growth rate on the (100) plane was one-tenth of that on the (010) and (310) planes. As explained by the authors, the adhesion energy on (100) terraces is lower than on other planes, so the re-evaporation rate of atoms supplied to the (100) terraces is higher than on other planes. Typical deposition temperatures were in the range of 600-900°C. Lower growth temperatures of 600-700°C were reported to provide smoother surface morphology for epitaxial films grown at high growth rate (0.7 μm/hr) [65].

2.7.5. Flux growth

Crystal growth from a melt flux is a well-known technique to produce crystals of various materials including oxides and complex oxides. With the use of a flux it is possible to reduce the growth temperature well below the melting point of the solute phase. Therefore the process conditions are milder compared to those used for the melt growth methods. For the most part the technique produces crystals of sizes and quality adequate for research purposes. Unfortunately, flux grown crystals are often contaminated by solvent, which makes their application for electronic devices difficult.

Gallium oxide crystals containing various amounts of rare-earth impurities (1.2 to 6.4 wt.% Sm_2O_3) were grown from various mixtures in the systems Ga_2O_3 Sm_2O_3-PbO/PbF_2 and Ga_2O_3 Sm_2O_3-MoO_3 [68]. In both systems large platelets of β-Ga_2O_3 single crystals were formed by a chemical decomposition process of $Sm_3Ga_5O_{12}$ in the presence of the PbO/PbF_2 or MoO_3 flux.

$$Sm_3Ga_5O_{12} \xrightarrow{\text{flux}} 3\,Sm_2O_3 + 5\beta\text{-}Ga_2O_3$$

The Sm_2O_3 is dissolved by the flux. The temperature of the process was ~1300 °C for PbO/PbF_2 flux and ~1050 °C for the MoO_3 flux. Chase and Osmer [69] reported on Ga_2O_3 growth with Bi_2O_3-PbF_2 flux. Standard 100 and 50 ml platinum crucibles were loaded with 20 mole % Ga_2O_3, 23 mole % Bi_2O_3, and 57 mole % PbF_2. These runs were heated to 1250 °C, held for 2 to 4 hours, and cooled at 4 °C/hr to 1000 °C. The crystals were normally 2 by 4 by 10 mm, and were extracted from the flux with hot 25% nitric acid. They were twinned and had many inclusions. The quality of the crystals was improved by blowing air directly at the bottom of the crucible and thus creating a temperature gradient across the crucible. In addition, this created a cold spot on the crucible where crystals first nucleated. Using this technique, clear rod-shaped crystals were produced and the frequency of the twinning was reduced. Garton et al. [70] studied flux growth of a variety of oxide crystals including β-Ga_2O_3. For the growth of β-Ga_2O_3 they used a Bi_2O_3-V_2O_5 flux. The addition of V_2O_5 greatly reduces the corrosive attack of the platinum crucible by Bi_2O_3 melt. A starting mixture of Ga_2O_3, Bi_2O_3, and V_2O_5 was loaded into platinum crucible and heated to 1300 °C and soaked for 14 hours to assure complete dissolution of the solutes. After that the crucible was cooled at the rate of 5 °C/hr to 900 °C. As a result, transparent, colourless β-Ga_2O_3 plates up to 6 mm edge were obtained. Ahman et al. [12] described growth of Ga_2O_3 crystals with a PbO-B_2O_3 flux. The mixture of Li_2CO_3, Ga_2O_3, PbO, and B_2O_3 was placed in a platinum crucible, heated to 200 °C and left for 2 hours at this temperature to remove moisture. Then the crucible was slowly heated up to 1250 °C and soaked at this temperature for 4 hours. After cooling to room temperature, the flux was removed with dilute nitric acid, yielding needle-shaped crystals up to 4 mm long.

2.7.6. Melt growth

Melt growth is the most viable and most frequently used technology to produce single crystals of various materials. As a rule, melt growth methods outperform all other techniques for crystal growth (from vapour, solution, etc.) in terms of higher growth rate, scalability and crystal quality. Gallium oxide does melt congruently at about 1820 °C in oxidizing environment. However, it decomposes into volatile lower oxides when heated under oxygen deficient atmosphere. The following decomposition reactions take place:

$$Ga_2O_3(l,s) \rightarrow 2\,GaO(g) + 1/2\,O_2(g),$$

$$2\,GaO(g) \rightarrow Ga_2O(g) + 1/2\,O_2(g),$$

$$Ga_2O(g) \rightarrow 2\,Ga(g) + 1/2\,O_2(g).$$

Thermal decomposition of β-Ga_2O_3 crystals becomes noticeable at temperatures above 1200 °C [71]. Evaporation of the melt disturbs the growth process and causes undesirable mass transport from hot to cold zones of the growth chamber. The formation of metallic gallium also poses a serious problem as liquid gallium is corrosive to all metals except niobium and tantalum. The decomposition of the melt can be suppressed under an oxygen-containing atmosphere. A small amount of oxygen (2% oxygen in 98% nitrogen) reduces the evaporation of the molten material drastically and almost no evaporated material is observed at the chamber walls [72].

The choice of a suitable crucible material, which can withstand the high melting point and corrosion attack of the melt, is rather limited. Under these conditions, most of refractory materials will be either oxidised or dissolved by the Ga_2O_3 melt. Iridium crucibles are conventionally used. The use of sapphire crucibles has been also reported in [73]. Alternatively, crucible-free techniques such as floating zone growth [24,74-79] and Verneuil method [70-

82] have attracted much attention from researchers. Verneuil method also referred to as flame fusion is one of the oldest methods to produce various crystals and gemstones. In this technique a fine powder of a source material is supplied into a flame of a downward pointing oxyhydrogen torch. The powder melts in the flame and forms a small puddle of a liquid phase on a seed crystal. The crystal is slowly lowered down allowing the base of the puddle to crystallize, while new melt is supplied by dropping powder through the flame. Long cylindrical crystals can be grown in such manner. The first attempts to adapt Verneuil method for the growth of Ga_2O_3 crystals were undertaken in 1960s by Chase [80]. The largest untwinned crystal fragment produced had a cross section of 2 by 8 mm and was 20 mm long. Lorenz et al. [81] reported on Ga_2O_3 flame fusion growth using an inductively couple plasma and oxygen-propane torches instead of a conventional oxyhydrogen flame fusion burner. The plasma torch with 20% oxygen-argon working gas provided an oxidizing growth atmosphere. The oxy-propane torch was used for the growth experiments under reducing conditions. Crystals grown under oxidizing conditions were transparent and colourless, while crystals grown in a reducing atmosphere were light blue. The boules were grown at a rate of approximately 10 mm/hr. Single crystal slabs up to 1.5 cm in the longest dimension could be cleaved from the boules. The major drawbacks of Verneuil method are high mechanical stresses induced during the growth and limited size of the crystals. This is especially critical in the case of Ga_2O_3 because of cleavage nature of the crystals. At present, Verneuil process is losing its importance in favour of more versatile techniques such as floating zone, Czochralski and edge defined film fed growth. However, this method is still viable to produce small Ga_2O_3 crystals for research purposes.

Recently, an optical floating zone technique has been employed for crystal growth of a wide range of materials, including metals, oxides, and semiconductors. In particular, this technique has attracted much interest as the method of choice for the growth of various nonconventional oxides including Ga_2O_3 [79]. A ceramic rod is placed in an optical image furnace equipped with halogen or xenon lamps and ellipsoidal mirrors focusing the light flux on a small area of the rod. The rod is locally melted establishing a liquid phase called a floating zone. After the floating zone is created it starts moving along the rod either by moving the mirrors up or by moving the rod. As the floating zone progresses along the rod, the polycrystalline source material melts and then solidifies into a single crystal. During growth feed and seed rods rotate either in the same or in opposite directions with experimentally established rates. The greatest advantage of the float zone technique is that no crucible is necessary. High quality crystals can be grown; however, their size is typically small.

A number of research groups have reported on Ga_2O_3 growth by the floating zone method [24,74-79]. More or less similar approaches have been employed in all studies. The feed rods were prepared from Ga_2O_3 powder by isostatic pressing and high temperature sintering. When necessary, doping impurities in the oxide form were introduced into the feed rods. Typical growth rates were in the rage from 5 to 15 mm/hr. The growth was conducted under oxidizing atmosphere such as pure oxygen [74], dry air [24,74] and controlled O_2/N_2 mixture [75]. In most cases crystals of few mm wide and several cm long have been grown. In contrast, Villora et al. [75] were successful in growing much larger Ga_2O_3 crystals up to 25 mm in diameter and 50 mm long. In the latter publication, authors presented an analysis of Ga_2O_3 growth with different oriented seed crystals. The identification of the stable growth orientations is determinant, first, for the growth of large-size crystals, and second, to obtain high-quality single crystals. It was found that the growth proceeded stable only when the (100) or the (001) cleavage planes were parallel to the growth axis, i.e. along <100>, <010> and <001> directions. Along these directions, the stress induced in the crystals during the growth at high temperatures was remarkably reduced, so that crystals could be grown more easily in single crystalline form, without cracks or twins. The authors explained this observation by the cleavage nature of the (100) and (001) planes of β-Ga_2O_3.

The Czochralski process also known as pulling crystal growth is a widespread method to produce cylindrical single crystals of various materials. The principle of the method is based on pulling of a single crystal ingot from a melt contained in a crucible. The main advantages of the Czochralski method are the fast growth rate, scalability to large diameters and good quality of single crystals. Iridium crucibles are commonly employed for the growth of high melting oxides. It is important to note that iridium is sensitive to oxidation especially at medium temperatures around 1200-1400 °C. At high temperatures iridium remains intact even at high oxygen concentrations due to its catalytic surface effect. The upper limit of the oxygen content in the growth chamber is about ~2-3 vol.%. On the other hand, oxidizing atmosphere is required to stabilize the melt

and prevent the decomposition of Ga_2O_3. Although free oxygen can efficiently suppress decomposition of Ga_2O_3, it is too aggressive towards iridium parts in the hot zone. As reported by Galazka et al. [71], 98% Ar + 2%O_2 at 1 bar pressure atmosphere provided sufficient O_2 concentration, but caused an extensive oxidation of all iridium parts at temperatures below 1200 °C.

An alternative approach is to replace free oxygen with carbon dioxide [72]. At high temperature CO_2 decomposes into CO and O_2. The partial pressure of oxygen increases with increasing temperature because the decomposition rate is enhanced at higher temperature. This amount of liberated oxygen is just sufficient to stabilise the Ga_2O_3 melt as well as low enough to prevent oxidation of iridium crucibles. Galazka et al. [71] reported on Czochralski growth of Ga_2O_3 crystals under different ambients. The following growth atmospheres have been tested: 50% Ar + 50% CO_2 at 1 bar, CO_2 at 7 bar and 98% Ar + 2% O_2 at 1 bar. The best results in terms of growth stability and crystal quality were obtained for the growth atmosphere 100% CO_2 at 7 bar, and the worst for 98% Ar + 2% O_2, which was due to extensive iridium oxidation. The measured evaporation rate of the volatile Ga_2O_3 species was 5 times lower for CO_2 / 7 bar than for 50% Ar + 50% CO_2 / 1 bar. The experimental results were in good agreement with thermodynamic calculations for the Ga_2O_3-CO_2-O_2-Ir system.

With the perfection of the technology, the size of Czochralski grown Ga_2O_3 crystals was steadily increasing from Ø10 mm by 20 mm in 2000 [72], to Ø18-22 mm by 40-65 mm in 2010 [23] to Ø50 mm by 75 mm in 2014 [14]. A crystal slab of two inches in diameter and 1 cm thick was successfully cut from a 3 inch long crystal produced by Czochralski method. As found in [14], Czochralski growth process remains stable if the free electron concentration is below 10^{18} cm^{-3}. Higher carrier concentration can result in spiral growth. This is explained by the strong dependence of the optical absorption in the Ga_2O_3 crystals on the free carrier concentration. High concentration of free electrons results in increased absorption in the near infrared region of the optical spectrum. In turn, this changes radiative heat transfer through the liquid–solid interface and then through the crystal. Heat absorption in the near infrared region causes convex-to-concave interface inversion which in turn can lead to a spiral formation. Doping with Mg also stabilizes the growth as Mg is an efficient compensating impurity and thus reduces the free electron concentration.

The edge defined film fed growth (EFG) technique uses a die which allows to precisely control the shape and dimensions of the crystal ingot. Ribbons, rods, fibres, tubes and more complex shapes can be produced. Because EFG technique can produce near net shape crystal ingots, the amount of post-growth machining and associated manufacturing costs can be significantly reduced. Shimamura et al. were the first group to demonstrate the growth of 2-inch size of β-Ga_2O_3 by the EFG method [83]. Later, EFG growth of β-Ga_2O_3 was reported by Aida et al. [84]. The quality of produced EFG crystals was studied by X-ray diffraction and etch pit density measurements. Typical full width at half maximum of (100) ω-scans was approximately 70-160 arcsec and the etch pit density was in 10^5 cm^{-2} range. Recently, Tamura Corporation (Japan) [85] started commercial production of β-Ga_2O_3 substrates using EFG technique. Ga_2O_3 substrates up to 2 inch in diameter are already commercially available. Larger substrates of 4 and 6 inch diameter are being developed by Tamura Corporation [86]. The crystalline quality of β-Ga_2O_3 crystals grown by the FZ and EFG techniques was compared in [87]. The (100) rocking curves for the FZ crystals showed several overlapping peaks of about 200 arcsec FWHM. In contrast, twin-free wafers can be produced by the EFG technique, exhibiting FWHM below 350 arcsec. The rocking curve of the best [$\bar{2}$01] wafer, with a FWHM was as narrow as 19 arcsec. Further, the etch pit density of these wafers was as low as 10^4 cm^{-2}.

2.8. Conductivity control and doping

Due to its wide bandgap, β-Ga_2O_3 is intrinsically an insulator. However, it also exhibits very good n-type conductivity when synthesized under reducing conditions. The n-type semiconductivity is commonly attributed to oxygen vacancies which are ionized and form donors. Conductivity of the Ga_2O_3 crystals grown by floating zone method can be controlled by changing the gas ambient or by doping. As reported by Uedaa and Hosono [77], the conductivity of Ga_2O_3 crystals could be controlled from 10^{-9} to 38 $\Omega^{-1}cm^{-1}$ by changing the oxygen content in the growth atmosphere. Highly insulating colourless crystals were synthesized in pure O_2 atmosphere. The conductivity of the crystals was below 10^{-9} $\Omega^{-1}cm^{-1}$ which was under the limit of the measurement. As N_2 gas was introduced, evaporation of the melt was accelerated, and the colour of the grown crystals became pale blue. The conductivity of the crystals was increasing with decreasing oxygen content. The

maximum conductivity measured was 38 $\Omega^{-1}cm^{-1}$ for a sample grown in a gas mixture with a pressure ratio of N_2/O_2 0.4/0.6. The growth was unstable under low O_2 conditions.

Similar correlation between the growth conditions and the conductivity was observed by Galazka et al. [14] for the Ga_2O_3 crystals produced by Czochralski method. In order to prevent decomposition of the Ga_2O_3 melt, the growth chamber was filled with Ar/CO_2 or pure CO_2 atmosphere. At high temperature CO_2 reversibly decomposes into O_2 and CO. Thus, CO_2 partial pressure controls the partial pressure of oxygen partial in the growth chamber. With increasing CO_2 partial pressure the colour of the crystals was changing from blue to colourless to grey. Transparent crystals had the lowest conductivity (<1 $\Omega^{-1}cm^{-1}$). The blue colouration was the result of the free carrier absorption, while the grey coloration could be due to possible carbon incorporation into the crystal lattice. An interesting observation is that the crystal grown under higher oxygen partial pressure (7 bar of pure CO_2 overpressure) revealed higher donor concentration, which contradicts the results reported for the floating zone method. Such behaviour of Ga_2O_3 can be explained by a reducing action coming from the decomposition of CO_2 [23]. The increased conductivity of the crystals grown under high CO_2 partial pressure can be also accounted for carbon contamination.

Because of strong correlation between conductivity of β-Ga_2O_3 crystals and oxygen partial pressure in growth or annealing environments, n-type conductivity was commonly attributed to the presence of oxygen vacancies. However, this assumption has been questioned by Varley and co-workers [21] who performed first-principle calculations based on hybrid functional theory of various impurities and oxygen vacancies in β-Ga_2O_3. According to these calculations, oxygen vacancy acts as a deep donor with ionization energy of more than 1 eV and thus cannot contribute to n-type conductivity. Authors suggested that hydrogen is the likely cause of the observed electrical conductivity in unintentionally doped β-Ga_2O_3.

Doping with other elements also affects the electrical conductivity and free electron concentration of β-Ga_2O_3 crystals. For example, group IV elements such as Si, Ge and Sn substituting on the Ga site or group VII elements such as Cl and F substituting on the O site act as shallow donors [21]. Si and Ge prefer the tetrahedral coordination of the Ga(I) site, while Sn prefers the octahedral coordination of the Ga(II) site. F and Cl both prefer the threefold coordination of the O(I) site.

Results on the floating zone growth of Sn doped Ga_2O_3 crystals were reported by Suzuki et al. [76] and Ueda et al. [77]. Highly conductive crystals were produced by floating zone method using Ga_2O_3 rods doped with 2-10 mol.% of SnO_2. Even though the crystals were grown under oxygen atmosphere, conductivity values of 0.96 $\Omega^{-1}cm^{-1}$ [77] and 56 $\Omega^{-1}cm^{-1}$ [76] have been reported. The incorporation efficiency was quite low because a vast amount of the Sn atoms in the feed rods evaporated during the crystal growth. As reported by Ueda et al., growth using feed rods with 3 mol.% of SnO_2 resulted in Ga_2O_3 single crystals with 0.05 % of Sn atoms. The values given by Suzuki et al. are almost an order of magnitude lower. In their experiments residual elemental Sn was found to be about 32–45 ppm, for the starting concentration in the feed rods of 2-10 mol.%. Nevertheless, the quantity of the remaining Sn atoms was still enough to provide concentration of free electrons in the range of mid 10^{18} cm^{-3}. The mobility was in the range 50-100 cm^2/Vs [76]. Ga_2O_3 crystals doped with SnO_2 had a blue coloration [77].

Silicon is another potential donor impurity in Ga_2O_3. The relative difference between atomic radii of Si^{4+} and Ga^{3+} is approximately -40%. This is significant compared to relative atomic radii differences for Ge^{4+} and Sn^{4+} which are -16% and +14%, respectively [88]. From the point of view of atomic radius, Ge^{4+} and Sn^{4+} accommodate better than Si^{4+} in the Ga^{3+} cationic site. However, Si has a higher potential as an n-type dopant for crystals grown from the melt, since it remains in the melt, while Ge and Sn evaporate to a high extent [88]. Villora and co-workers [88] produced Si doped Ga_2O_3 crystals by floating zone method. The feed rods were prepared by a sintering process from a mixture of SiO_2 and Ga_2O_3 powders with concentration of Si varying from 0 to 0.2 mol %. The resulting Si concentration in the β-Ga_2O_3 single crystals was in the range from 10^{16}-10^{18} cm^{-3}. At low-doping levels, almost all Si incorporates into the crystal, while at high-doping levels the concentration of Si in the crystal is about 5% of that in the feed rod. The conductivity continuously increased with increasing Si concentration in the feed rod, from a value as low as 0.03 $\Omega^{-1}cm^{-1}$ for nominally undoped crystals to 50 $\Omega^{-1}cm^{-1}$ for highly doped crystals. It was found that while the mobility fluctuated around 100 cm^2/Vs, the free-carrier concentration systematically increased with the silicon concentration by over three orders of magnitude, 10^{16}–10^{18} cm^{-3}. Since Si is found to be the main impurity in correlative concentrations in commercially available Ga_2O_3 powders, the phenomenon of electrical conduction can be linked to Si doping,

and the attribution to ionized oxygen vacancies is no longer sustainable. This is well in line with theoretical calculations [21] showing that oxygen vacancies in β-Ga_2O_3 are deep donors and cannot be responsible for electron conductivity in β-Ga_2O_3 crystals.

Interesting results on Si-ion implantation into Ga_2O_3 crystals synthesized by the floating zone method were published by Sasaki et al. [89]. The total dose was varied from $2{\cdot}10^{14}$–$2{\cdot}10^{15}$ cm^{-2}, corresponding to Si concentrations from $1{\cdot}10^{19}$–$1{\cdot}10^{-20}$ cm^{-3}. For $Si^+ \leq 5{\cdot}10^{19}$ cm^{-3} a high electrical activation efficiency above 60% was obtained after annealing at a relatively low temperature of 900–1000 °C. The lowest resistivity value of 1.4 mΩ cm was obtained for the sample with $Si^+ = 5{\cdot}10^{19}$ cm^{-3}.

Gogova et al. [55] have grown thin films of β-Ga_2O_3 doped with Si on Al_2O_3 (0001) and β-Ga_2O_3 (100) substrates by metal organic vapour phase epitaxy. Trimethylgallium (TMG) and water vapours were used as gallium and oxygen precursors. Tetraethylorthosilicate (TEOS) was used as a silicon source. The growth temperature was in the range 800-850 °C. SIMS investigations showed that Si may be incorporated up to about $5{\cdot}10^{19}$ cm^{-3} but Hall and CV measurements confirmed a very low conductivity of both as-grown and annealed films.

Attempt to produce Ge-doped Ga_2O_3 polycrystalline material using conventional ceramic techniques were undertaken by Nag and Shireen [90]. A mixture of Ga_2O_3 and GeO_2 was ground, pelletized and fired at high temperature. Then the pellets were reground, re-pelletized and fired again. The process was repeated three or four times with successively increasing temperatures in each firing round from 1150 °C to 1400 °C. Produced samples were optically transparent in the visible range and consisted of a single phase containing ~3.5% of Ge. However, the samples exhibited insulating behaviour with a resistivity of the order of a few tens of MΩ·cm. It is likely that the temperature of the process was not sufficient to achieve activation of Ge donors.

As reported by a number of authors, magnesium doping results in insulating β-Ga_2O_3 crystals. Onuma et al. [34] have grown Mg-doped β-Ga_2O_3 crystals by the floating zone technique. The samples exhibited a semi-insulating behaviour, and resistivity of $6{\cdot}10^{11}$ Ωcm was obtained with a Mg concentration of $4{\cdot}10^{18}$-$2{\cdot}10^{19}$ cm^{-3}. Galazka et al. [14] found that Czochralski grown β-Ga_2O_3 crystals doped with Mg in a very low range of 6–28 wt. ppm were insulating when grown at 100% of CO_2, indicating that Mg is a very efficiently compensating acceptor. In addition to that, Mg-doping was found to stabilize the growth and reduce the probability of the spiral formation. The equilibrium segregation coefficient of Mg across the liquid-solid interface during growth of β-Ga_2O_3 single crystals by the Czochralski method was estimated to be 0.1 - 0.12. Feng et al. [91] found that high Mg doping changes the bandgap of Ga_2O_3 films grown on MgO substrates by MOCVD. The bandgap monotonously increased with increasing Mg concentration. Optical bandgaps for the 1%, 3%, 5%, 7%, and 10% Mg-doped Ga_2O_3 films were 4.93, 5, 5.09, 5.21, and 5.32 eV, respectively. After annealing, the absorption edge of all the films shifted to the longer wavelengths, with optical bandgaps of 4.87 eV, 4.93 eV, 5.04 eV, 5.1 eV, and 5.22 eV obtained for the samples with Mg concentrations of 1%, 3%, 5%, 7%, and 10%, respectively. The dependence of the bandgap on the Mg content can be ascribed to the formation of MgO-Ga_2O_3 alloy, as MgO has a larger band gap of 7.8 eV.

The possibility of p-type conductivity in Ga_2O_3 remains controversial. So far there are no reports on clear hole conduction in p-type Ga_2O_3. Liu et al. [92] claimed to have produced nitrogen doped Ga_2O_3 nanowires with p-type conductivity. The authors have drawn the conclusion of p-type conductivity based solely on I-V measurements; no in-depth analysis on the carrier mobility and concentration has been given. Theoretical modelling by Zhang and co-workers [19] revealed that nitrogen forms a shallow acceptor impurity level at the top of the valence band with the Fermi level intersecting the impurity level.

Tomm et al. [74] reported on p- and n-type conductivity in Ge- and Ti-doped Ga_2O_3 single crystals produced by the floating zone technique. However room-temperature hole concentrations were in the range of several 10^5 cm^{-3}, which is far too low for any practical applications.

According to other theoretical calculations [33], p-type conductivity in β-Ga_2O_3 is rather impossible because of strong self-localisation of holes. This localization is due to the ionicity of metallic oxides. A positive hole, if it is successfully introduced by substitutional doping, for instance, localizes on a single oxygen atom and cannot migrate within the crystal lattice, even under an applied electric field [93]. Therefore, very low hole mobility in the order of 10^{-6} cm^2/Vs is expected at room temperature. Such a low value indicates that, even if holes could be introduced in Ga_2O_3, no significant p-type conductivity can be achieved.

3. APPLICATIONS

3.1. Catalysis

Gallium oxide has been reported to have catalytic activity for various chemical reactions including catalytic combustion, CO oxidation, NO_x's selective reduction, etc. The catalytic activity of Ga_2O_3 has been attributed to the unique structural characteristics of coordinatively unsaturated surface Ga^{3+} cations, which is believed to be crucial for hydrocarbon activation in CO_2 atmosphere. Catalytic properties of Ga_2O_3 are strongly influenced by polymorphism. Catalytic activity of β-Ga_2O_3 was the highest among other polymorphs in reactions such as dehydrogenation of propane to propene [94] and oxidation of hydrocarbons [95]. The γ-Ga_2O_3 polymorph is of particular interest for potential applications in heterogeneous catalysis because of its high surface area of 120 m^2g^{-1} [96]. As it has been pointed out by Zheng et al. [94], the reactivity of the polymorphs correlates with the surface acidity, therefore it can be concluded that the surface acid site density probably plays a decisive role in catalysis. It is known that tetrahedral Ga ions exist in the structure of β- and γ-Ga_2O_3, and surely they are the source of the Lewis acidity. By contrast, α- and δ-Ga_2O_3 are constituted only by octahedral Ga^{3+}, and theoretically the formation of Lewis acid sites on these oxides is unlikely. β-Ga_2O_3 is the most active catalyst because it has the highest surface acid site density, whereas the activities of the other three polymorphs are similar but lower, because of their reduced surface acid site density.

Gallium oxide exhibits strong photocatalytic activity. When irradiated by UV light, electron–hole pairs are generated. The holes can react with water molecules to give hydroxide radicals (OH) and the electrons can produce superoxide (O^{2-}). Depending on the reaction conditions, the holes, OH radicals, O^{2-}, H_2O_2, and O_2 can play important roles in the photocatalytic reaction mechanism. The advantages of the photocatalytic process are that it can be conducted at room temperature and is cost-effective, efficient, and environmentally friendly. When compared to conventional photocatalysts such as TiO_2, Ga_2O_3 has much wider band gap, therefore photogenerated electrons in the conductive band have much higher reductive capability. The band-edge potentials of the conduction and valence band were found to be at 1.1 V higher and 2.5 V lower than H^+/H_2 and O_2/H_2O redox potentials [97]. The relatively large overpotentials make Ga_2O_3 an attractive material for photoelectrolysis of water [37,98]. Ga_2O_3 can be used for oxidation and mineralization of organic compounds and pollutants. Hou et al. [95] tested photocatalytic activities of various Ga_2O_3 polymorphs for the decomposition of volatile aromatic compounds (e.g., benzene, toluene, and ethylbenzene). It was found that the Ga_2O_3 catalysts exhibited much higher photocatalytic activity than commercial TiO_2. Among all other polymorphs, β-Ga_2O_3 exhibited the highest specific photocatalytic activity.

Ga_2O_3 nanostructures have recently drawn growing attention in catalysis and photocatalysis applications because of their large surface-to-volume ratio, which provides more surface sites which can interact with environment. The abundance of gap states naturally existing inside the nanostructures increases light absorption and thus the efficiency of the photochemical reaction. Catalytic ability of Ga_2O_3 nano/microstructures such as belts [99] , wires [100], rods [101], microspheres [102] have been studied. Li and co-workers [103] reported on enhanced photocatalysis in Ga_2O_3 photonic crystals through intensifying electronic band absorption.

3.2. Phosphors and electroluminescent devices

Gallium oxide has gained attention as a new phosphor host material for emissive display applications such as thin-film electroluminescent displays, field-emission displays, plasma display panels and fluorescent lamps. Conventional sulphide based phosphors have many disadvantages such as the lack of primary colour emissions and chemical instability, especially in regard to moisture. In contrast, gallium oxide is very stable both chemically and physically. Because of high electric strength of Ga_2O_3, it is possible to apply higher electric fields to the Ga_2O_3 electroluminescent devices. Ga_2O_3 activated with transition metals, rare-earths or other elements exhibits strong luminescence emissions at various wavelengths. Gallium oxide doped with manganese [104] and europium [105,106] are of particular interest because these dopants produce green and red emissions which are suitable as primary colours in full-colour displays. Doping with Mn results in a broad emission peak centred at around 500 nm [47,107]. Yellow and blue emission colours can be also obtained using Ga_2O_3 phosphors activated with Ce, Tm or Sn and Dy, respectively [107].

Trivalent rare earth ions are isovalent impurities in Ga_2O_3, which is beneficial for electroluminescent devices. According to Wager et al. [108], when the luminescent impurity is a donor or acceptor, it strongly perturbs space charge neutrality, leading a

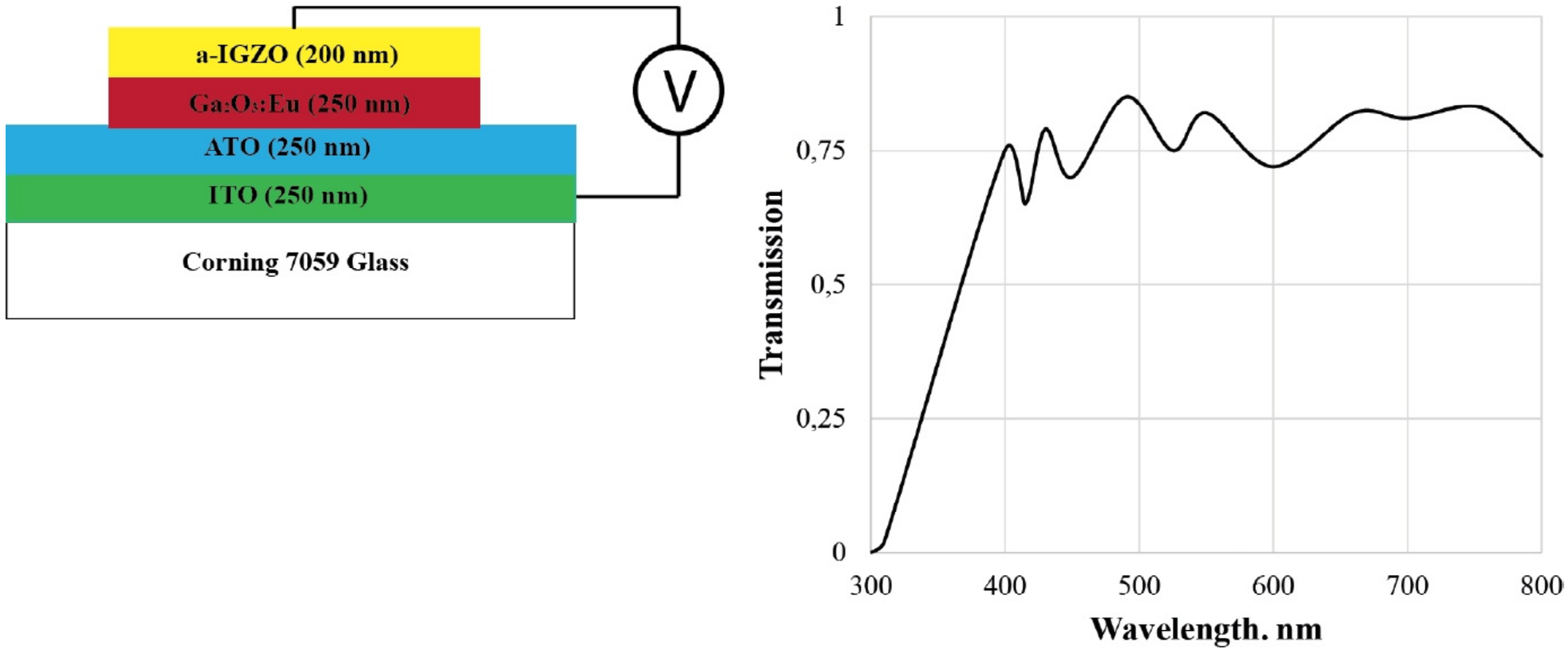

Fig. 4. Left: A schematic diagram of the thin film electroluminescent (TFEL) device structure as deposited by PLD onto the ATO/ITO/glass substrate. Right: Transmission spectrum of the complete device stack showing about 70% transparency throughout the visible region of the spectrum. According to the description from Ref. [111].

wide bandgap phosphor to resort to self-compensation, and thus introducing new electronic states into the bandgap. In turn, this results in non-ideal characteristics of an electroluminescent device. The unique luminescent properties of trivalent rare earth dopants are better manifested in the host materials with a group III cation such as Ga_2O_3.

Green phosphor with emission line at 543 nm can be produced by terbium doping [109]. Gallium oxide doped with europium was found to be a bright red phosphor [35,44,110,111]. When doped with Eu^{3+} and Tb^{3+} together, gallium oxide nanoparticles emit white light [112,113]. Bright blue, green and red emissions are generated due to host material (Ga_2O_3), Tb^{3+}, Eu^{3+}, respectively. The mixture of these emission lines is perceived as a white light with chromaticity coordinates (0.33, 0.33) [112] or (0.32, 0.36) [113] which falls well in the white region of the CIE chromaticity diagram.

3.3. Gas sensors

Many Ga_2O_3-based gas sensors have been investigated. Oxygen sensors utilize the fact that the conductivity of β-Ga_2O_3 n-type polycrystalline films is inversely proportional to the oxygen partial pressure in the surrounding ambient. At high temperatures β-Ga_2O_3 has an oxygen deficiency in the crystal lattice that is in dynamic equilibrium with the oxygen in the surrounding atmosphere. Variations in the conductivity of the sensor are caused by variations of the concentration of ionized oxygen vacancies. Therefore, a reduction in the proportion of oxygen or an increase in the concentration of reducing gases in the atmosphere in which the sensor is located leads to an increasing number of conducting electrons and, hence, an increasing conductivity [114]. The linearity between the sensor conductivity and the oxygen content is held for partial pressures above 10^{-10} Pa. For lower partial pressures the conductivity decreases abruptly by several orders of magnitude. Fleischer and co-workers [114] suggested that β-Ga_2O_3 undergoes a phase transition at very low oxygen pressures, however they have not succeeded in identifying the new phase.

At temperatures around 600 °C, the oxygen sensitivity of polycrystalline Ga_2O_3 diminishes significantly and the films can instead be used to detect reducing gases such as hydrogen. As found by Fleischer and co-workers [115], in the temperature range 400-600°C the conductance of these films depends reversibly, according to a power law $\sigma_{\square} \sim \sqrt[3]{P_{H_2}}$, on the partial pressure of hydrogen in the ambient atmosphere of the Ga_2O_3 film. The authors concluded, that the H_2-induced changes in the electrical conductance of β-Ga_2O_3 result from reversible chemisorption of the hydrogen on the whole surface of grains of the polycrystalline Ga_2O_3 with subsequent electron transfer from the adsorbed hydrogen to the Ga_2O_3.

Another type of hydrogen sensor based on Ga_2O_3 Schottky diode structures was suggested by Trinchi et al. [116]. First, 90 nm of Ga_2O_3 was deposited by spin-coating on n-type 6H-SiC substrates using a sol-gel process. After that, a platinum Schottky contact of thickness 70 nm was deposited on top of the film by dc magnetron sputtering. It

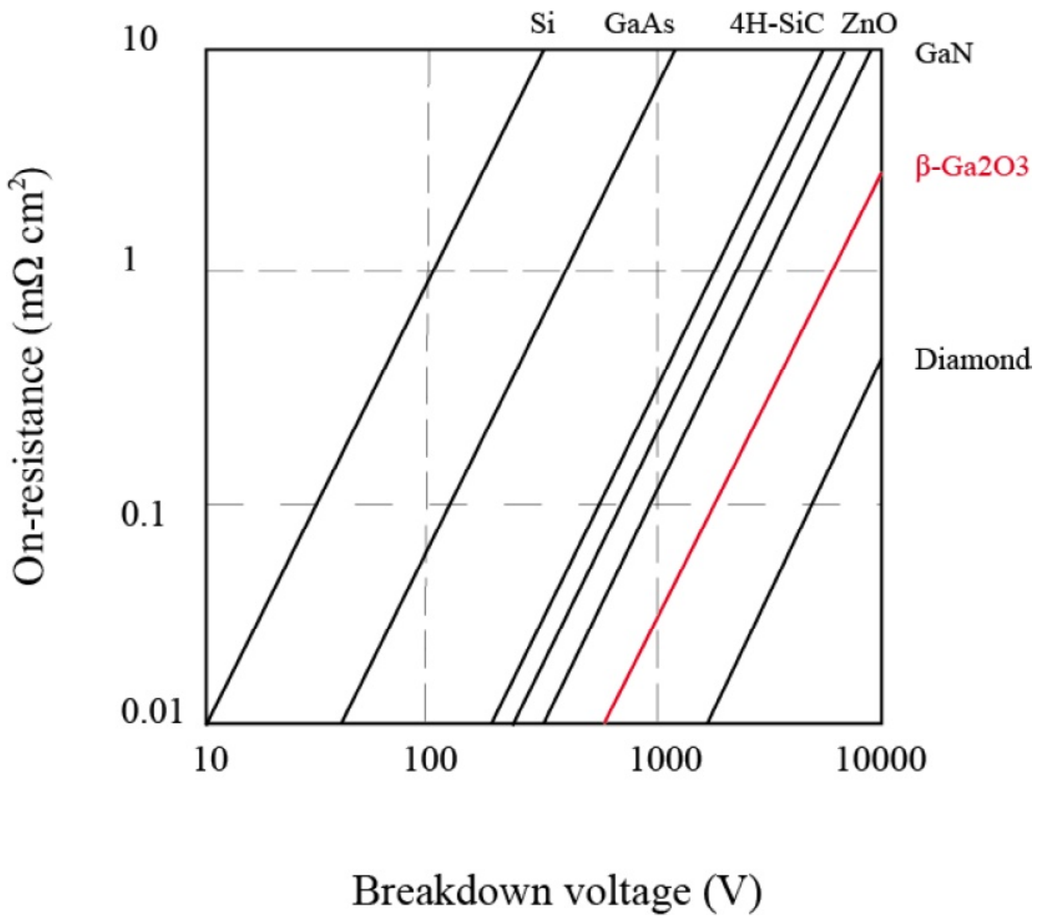

Fig. 5. Theoretical limit of on-resistance as a function of breakdown voltage for major semiconductors and β-Ga_2O_3. According to the description given in Ref. [64].

was found that introduction of hydrogen gas results in reduction of the Schottky barrier height at the Pt-Ga_2O_3 interface and the shift in the measured I–V characteristics. A nearly linear relation between the Schottky barrier height shift and the hydrogen concentration was obtained. When compared to conductance type hydrogen sensors, Schottky diode sensors offer much greater relative shift in sensor output and much faster response. Similar type of hydrogen sensors was studied by Nakagomi and co-workers [117]. They fabricated Pt/Ga_2O_3/SiC structures on n- and p-type SiC substrates. Both sensors had a large response. The sensors could detect 40 ppm hydrogen for certain under 20% O_2/N_2 at 500 °C under appropriate bias conditions.

It should be pointed out that the response of Ga_2O_3 sensor towards reducing components like ethanol or propane cannot be neglected in comparison with the oxygen response even at high temperature of 800 °C [40]. The cross-sensitivity to reducing components can be suppressed by additional catalytic or filter layers. For example, Ga_2O_3 sensors covered with nickel oxide have no response to methane at high temperatures. Dense silicon dioxide coating decreases sensor response to all reducing gases except hydrogen.

Gas sensors based on polycrystalline Ga_2O_3 films are efficient only at elevated temperatures. At low temperatures oxygen vacancies become frozen within the material. Although gas sensing can occur at these lower temperatures, it is limited to interactions at oxygen defect sites at the material surface. To overcome this limitation it is desirable to dramatically increase the available surface area for sensor/analyte interaction. This can be accomplished through the use of nanomaterials. Arnold et al. [118] demonstrated gas sensors based on Ga_2O_3 nanowires. The sensors had a rapid, reversible response at room temperature to acetone and methanol, and a more limited response to some hydrocarbons such as toluene.

For a more comprehensive review on gas sensors based on various oxide materials including Ga_2O_3 please refer to the publications of Moos et al. [40] and Fleischer [119].

3.4. Power and high voltage devices

Gallium oxide is a promising material for power and high voltage electronic devices. The bandgap of Ga_2O_3 is much larger than those of SiC and GaN. The critical electric field can be estimated from the bandgap using an empirical relationship [120]:

$$E_c = 1.73 \times 10^5 (E_g)^{2.5}. \quad (1)$$

This estimation results in the value of the critical field over 8 MVcm^{-1}, which is three times larger than that of either SiC or GaN. The potential of a semiconductor material for high power device applications can be estimated by Baliga's figure of merit (FOM) [121], which describes the resistive losses of a device.

$$\text{BFOM} \propto \varepsilon\mu E_c^3. \quad (2)$$

Baliga's FOM is proportional to the cube of the breakdown field, but only linearly proportional to the electron mobility and dielectric constant. Therefore, Baliga's FOM of β-Ga_2O_3 is at least four times larger

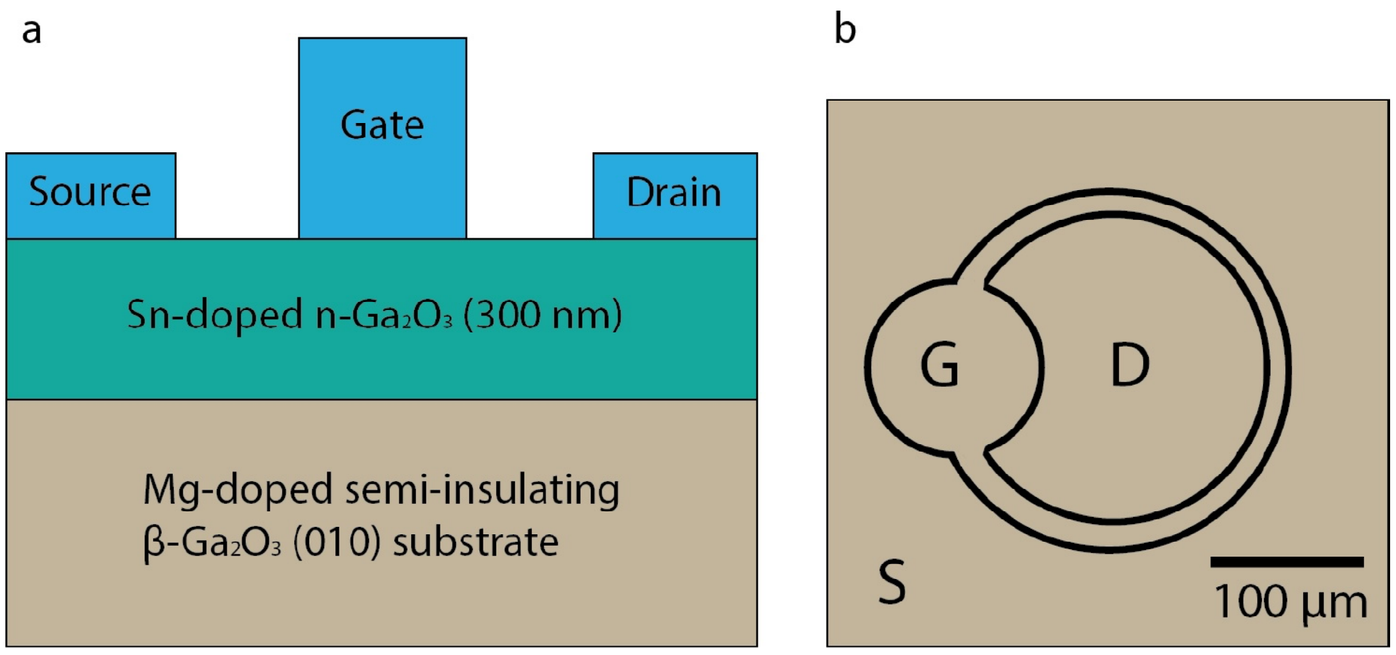

Fig. 6. Schematic illustration: cross-sectional (a) and top-view (b) of Ga_2O_3 MESFET. According to the description from Ref. [64].

than those of SiC or GaN. Fig. 5 shows theoretical limit of on-resistance vs breakdown voltage for Ga_2O_3 and representative semiconductors. As it can be seen, Ga_2O_3 is second only to diamond and outperforms Si, GaN, and SiC. However, it should be mentioned that Ga_2O_3 has very poor thermal conductivity (10.9-27 W/mK) compared to Si (130 W/mK) GaN (~150-200 W/mK) and SiC (360-490 W/mK). This is a clear weak point of Ga_2O_3 in terms of power device applications.

3.5. Schottky diodes

Sasaki et al. [122] reported on fabrication of Schottky diodes on β-Ga_2O_3 on (010) substrates. The Schottky contact was formed on the front side of the substrate as anode electrodes using standard photolithography patterning, Pt(15 nm)/Ti(5 nm)/Au(250 nm) evaporation, and liftoff. The back side of the wafer was etched by RIE in BCl_3 (35 sccm) and Ar (5 sccm) plasma. After that Ti (20 nm)/Au (230 nm) contact was evaporated. The RIE treatment changes the electrode properties from Schottky to ohmic and significantly decreases the contact resistance. A good ideality factor close to 1.0 has been demonstrated. The Schottky barrier height of the Pt/ β-Ga_2O_3 interface was estimated to be about 1.3–1.5 eV which is comparable with those of Pt/ SiC and Pt/GaN. The reverse breakdown voltage was up to 150V. This value is reasonably high since the devices had a simple structure without passivation or edge termination. Oishi et al. [123] fabricated high-performance Schottky barrier diodes on edge-defined fed-grown (201) β-Ga_2O_3 single crystals. The crystal plate was of 7.0×7.0 mm^2 area and 606 µm thickness. First, ohmic contacts were formed on the top surface of a β-Ga_2O_3 (201) single crystal. Next, Schottky contacts of Ni-Au metals were evaporated in circular shapes of 318 µm diameter on the top surface of the β-Ga_2O_3 single crystal. The current density for the forward voltage was 70.3 A/cm^2 at 2.0 V, and a nearly perfect ideality factor of 1.01 was obtained.

Most recently, properties of Au/ β-Ga_2O_3 Schottky diodes were analyzed both theoretically and with the use of computer modelling [124]. It was demonstrated that Schottky barrier height for Au/ β-Ga_2O_3 is 1.23 eV and threshold voltage is ~0.6 V under ~1µA current. Comparative analysis of the properties of Schottky diode Au/ β-Ga_2O_3 and devices based on various wide bandgap semiconductors including 4H-SiC, GaN and AlGaN has been done. It was shown that Schottky diode Au/ β-Ga_2O_3 had smaller reverse current than Au/GaN and Ni/4H-SiC. Calculated breakdown voltage for Au/ β-Ga_2O_3 Schottky diode was ~2500 V.

3.6. Field effect transistors

Matsuzaki et al. [39] fabricated top-gate MISFETs using the as-deposited Ga_2O_3 films grown on sapphire substrate for an n-channel layer and amorphous alumina for a gate insulator. The transistor operated under depression mode with a threshold voltage of 6.7 V and a saturation field-effect mobility of $5 \cdot 10^{-2}$ $cm^2V^{-1}s^{-1}$. The small mobility may be due to the granular structures of the film surface, difference in the crystal structure, and gate structure. Sasaki et al. [62,64] fabricated n-channel Ga_2O_3 MESFETs on a single-crystal β-Ga_2O_3 (010) substrate. A Sn-doped n-type Ga_2O_3 layer with a thickness of 300 nm was grown by MBE on a Mg-doped semi-insulating β-Ga_2O_3 (010) substrate fabricated by the floating zone method. Ohmic contacts were formed using a reactive ion etching treatment in BCl_3 and Ar plasma for 1min, followed by evaporation of Ti(20 nm)/Au(230 nm) and lift off. The RIE treatment significantly reduced the contact resistance.

Schottky gates were fabricated by Pt(15 nm)/Ti(5 nm)/Au(250 nm) deposition and lift off. A cross-sectional schematic illustration of the Ga_2O_3 MESFET structure are shown in Fig. 6. The breakdown voltage at the off-state was as high as 257 V at V_{GS}=-30 V. Note that the breakdown was catastrophic, resulting in burned gate electrodes. The maximum transconductance was 1.4 $m\Omega^{-1}$ at a drain bias of 40 V. The off-state drain leakage current was as small as 3 mA, and the on/off drain current ratio reached a high value of around 10,000.

An interesting design of a nanomembrane field effect transistor was developed by Hwang et al. [125,126]. As reported by the authors, β-Ga_2O_3 nanomembranes could be mechanically exfoliated from the bulk crystals, similar to the exfoliation of graphene and other layered crystal materials. The ease of exfoliation could be attributed to a much larger lattice constant in the (100) direction. Exfoliated Ga_2O_3 nanomembranes were transferred onto a P+ silicon substrate covered with 285 nm of thermal oxide on the front surface. The gate contact was deposited on the back surface of the Si substrate. The source and drain contacts were defined by electron beam lithography using Ti/Au (5/150 nm) metal stacks. The final device went through an annealing process in Ar/H_2 at 300 °C for three hours to reduce the contact resistance. Nanomembrane β-Ga_2O_3 FETs show a high gate modulation of 10^7 even under a high drain voltage of 20 V; this modulation is limited not by the channel material, but the gate leakage current. The high current modulation is attractive for high-power and high-voltage device applications. Field-effect mobility extracted from the transfer characteristics was of 70 cm^2/Vs. The contact resistance was measured to be 55 Ωmm at low V_{DS} which is much higher than that of conventional Si and III-V FETs of 0.1 Ωmm. The high contact resistance was responsible for the lower-than-expected on-current for a long-channel FET of similar geometry and transport properties. When corrected to contact resistance, the real mobility was estimated to be around 130 cm^2/Vs. The output characteristics of the nanomembrane β-Ga_2O_3 maintain a robust current saturation up to 70 V with no signs of output conductance.

Although the described method has limited scalability because mechanical exfoliation can produce only small area nanomembranes, the concept itself is rather interesting. It allows to circumvent poor thermal conductivity of Ga_2O_3 by employing materials with high thermal conductivity, such as CVD diamond of AlN ceramic, as a host substrate for Ga_2O_3 nanomebrane. Methods similar to smart-cut technology used in silicon-on-insulator wafer manufacturing can potentially enable controlled release of large area nanomembranes of Ga_2O_3 and thus make the technology more suitable for mass-production. The first prototypes of gallium oxide transistors are still inferior to the far more mature, SiC and GaN devices of today, however they have great potential. Gallium oxide transistors deliver comparable or better performance when benchmarked against first GaN MESFETs of the early 1990s.

3.7. Substrates for III-nitrides epitaxy

Despite recent progress in bulk growth of GaN single crystals, native GaN substrates remain costly and difficult to obtain. For that reason, the majority of gallium nitride devices are produced by heteroepitaxial growth on foreign substrates such as sapphire, silicon or silicon carbide. The growth on sapphire is well established, however insulating nature of sapphire makes it impossible to produce devices with vertical geometry. Even though SiC is conductive, it is expensive and has high optical absorption in the blue region of the spectrum. Silicon substrates also have many disadvantages such as large thermal and lattice mismatch, opaqueness in visible and UV spectra, chemical interaction with GaN in the growth environment, etc. Monoclinic β-Ga_2O_3 is a good candidate as a substrate material for the growth of III-nitrides, as it combines the advantages of transparent and conductive substrate. Moreover, high quality bulk Ga_2O_3 crystals can be produced by melt-growth techniques such as Czochralski and EFG at low cost and high throughput.

The first demonstration of MOCVD growth of GaN epilayers and device structures on (100) β-Ga_2O_3 substrates was by Shimamura et al. [127]. The deposition process was similar to that used for GaN growth on sapphire. First, a thin low-temperature nucleation layer was deposited at 600 °C. Then a GaN layer of 1000 nm was grown at 1070 °C. As a result, (0001) oriented wurtzite GaN with very smooth surface morphology have been produced. The x-ray rocking curve exhibited a full width at half maximum (FWHM) of 1200 arcsec which is rather wide compared to that for GaN layer grown on sapphire. In the same article authors also reported on fabrication of GaN/InGaN blue light emitting diodes having vertical chip design on Ga_2O_3 substrates. Similar results were published by Xie et al. [128] who demonstrated fabrication of GaN-based green light emitting diodes on (100) Ga_2O_3 substrates.

Ito et al. [129] employed a well-known facet-control MOCVD growth to improve the crystalline quality of GaN and AlGaN films on (100) Ga_2O_3 substrates. The basic idea of this approach is to change growth conditions in a way which favours the formation of inclined facets on the growth surface. Dislocations existing in the facet regions bend and do not glide to the surface. By applying this technique to GaN growth on Ga_2O_3 substrates, the aforementioned authors reduced the threading dislocations density by almost one order of magnitude.

MBE growth of GaN on (100) Ga_2O_3 substrates was reported by Villora et al. [130,131]. It was found that nitridation of Ga_2O_3 in ammonia is an important prerequisite for the growth of wurtzite GaN layer. The nitridation with ammonia, NH_3, starts to be effective at temperatures and pressures over 800 °C and 10^2 Pa, respectively. All attempts to nitridize Ga_2O_3 under N_2 gas or nitrogen radicals were in vain. Initial X-ray diffraction measurements [130] pointed to the alignment along main directions given by the epitaxial relationship: $\langle 010 \rangle_{\beta-Ga_2O_3} \| \langle 11\bar{2}0 \rangle_{GaN}$ and $\langle 001 \rangle_{\beta-Ga_2O_3} \| \langle \bar{1}100 \rangle_{GaN}$. However, more detailed TEM analysis indicated the preferential alignment along the diagonal, which is only about 1° tilted from the initial assignment. The epitaxial relationship is given by $\langle 011 \rangle_{\beta-Ga_2O_3} \| \langle 10\,\bar{1}0 \rangle_{GaN}$ [131]. The latter alignment is energetically more favourable because the small rotation of the GaN lattice reduces the lattice mismatch from ~5% to 2.6%. Moreover, for this configuration the in-plane lattice expansion of both β-Ga_2O_3 and GaN is very similar, so that the stress induced to the epitaxial layer during the cooling process to room temperature is minimal [87].

HVPE growth of GaN on Ga_2O_3 substrates has been demonstrated by Nikolaev et al. [132]. Ga_2O_3 platelets with (100) orientation were produced by cleaving of the β-Ga_2O_3 ingot. The surface of GaN layers is full of three-dimensional features such as faceted pyramids and pits. The full width at half maximum (FWHM) of the X-ray rocking curve is 546 arcsec. The quality of GaN epitaxial films was somewhat inferior when compared to that of GaN films grown on sapphire under optimized conditions which can be related to non-optimized growth conditions and defects in the β-Ga_2O_3 substrate. Kachel et al. [133] published on GaN growth on (100) β-Ga_2O_3 substrates using pseudo-HVPE technique. In this approach, hot ammonia in contact with carbon at 1050 °C forms HCN gas. The HCN reacts with gallium in the crucible at 1100 °C to form GaCN, which is transported by nitrogen carrier gas flow to the substrate, where the reaction with NH_3 occurs and GaN is formed. First, the substrate was annealed under NH_3 gas at 800 - 1000 °C to form a thin GaN buffer layer on the substrate surface [134]. Then the temperature was increased to 1000 - 1200 °C and thick GaN was grown. After cooling down to room temperature GaN layers self-separated from the Ga_2O_3 substrate which was facilitated by cleavage nature β-Ga_2O_3. Estimated dislocation density of GaN on Ga_2O_3 substrates, was in the range of 4.6×10^9 cm^{-2}.

While early publications on GaN epitaxial growth on β-Ga_2O_3 were focused on the growth on *a*-plane (100) substrates, there is increasing interest in the GaN growth on $(\bar{2}01)$ β-Ga_2O_3 substrates. Growth on (100) β-Ga_2O_3 substrates is complicated by the cleavage nature of the (100) plane, which causes the striping of the epi-layer and substrate. In contrast, growth on $(\bar{2}01)$ substrates is free of this problem. Muhammed [135] reported on MOCVD growth of wurtzite GaN on $(\bar{2}01)$ β-Ga_2O_3 substrates. The epitaxial relationships were defined for crystallographic planes as $\langle 010 \rangle_{\beta-Ga_2O_3} \| \langle 11\bar{2}0 \rangle_{GaN}$ and $\langle \bar{2}01 \rangle_{\beta-Ga_2O_3} \| \langle 0001 \rangle_{GaN}$ leading to a lattice mismatch of ~4.7%. The GaN lattice parameters, determined by the Bond method, showed a slight compressive strain.

MOCVD growth of high brightness InGaN light emitting diodes on $(\bar{2}01)$ β-Ga_2O_3 substrates was reported by KOHA Co., Ltd. & Tamura Corp [87]

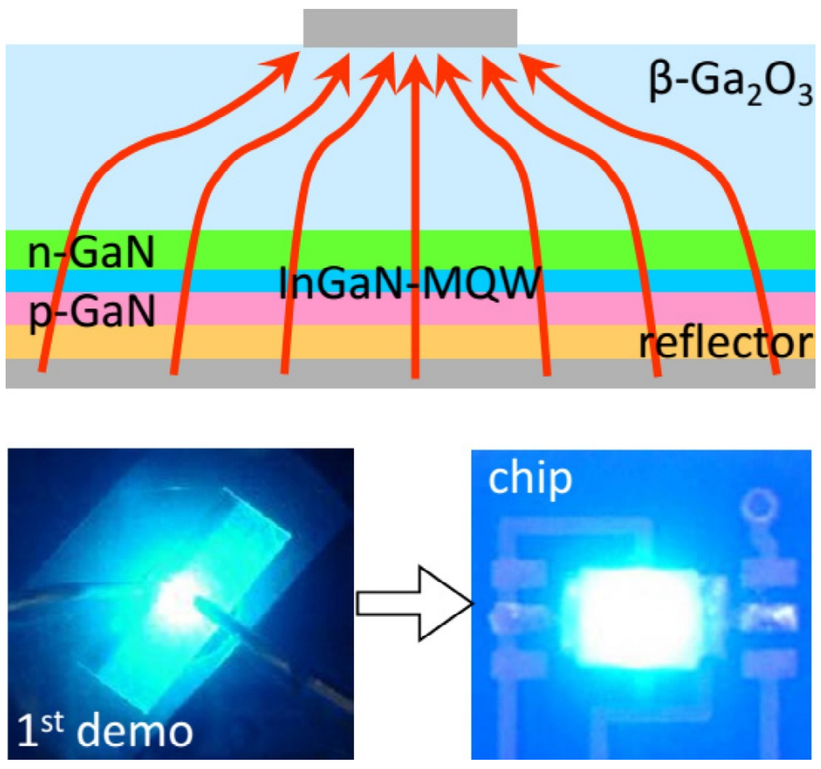

Fig. 7. Schematic of a blue-LED based on an InGaN-MQW deposited on a β-Ga_2O_3 substrate. Photograph of the initially demonstrated blue emission by vertical current injection in comparison with a current chip. Reprinted with permissions from E.G. Víllora, S. Arjoca, K. Shimamura, D. Inomata and K. Aoki // *Proc. of SPIE* **8987** (2014) 89871U, © 2014 SPIE.

(see Fig. 7). For a blue emission peaking at 447 nm, the forward voltage at 20 mA is as low as 2.96 V. This indicates that the series resistance is lower than on other substrates and therefore the heat losses are notably suppressed. The radiant flux for small area chips of 300×300 μm^2 was 360 mW at 650 mA. Large area chips of 2×2 mm^2 provided the radiant flux of 4.82 W at 10 A.

4. SUMMARY

This review summarises the research-to-date in the study of the gallium oxide as a perspective functional material for various applications including semiconductor devices, optoelectronics, catalysis, chemical sensors and many others. Among them, the most topical research area of the last decade was exploration of Ga_2O_3 as a new wide band gap material. Much of the research and development effort has been undertaken to achieve the high standards of purity and defect density required for the semiconductor applications. To date, a significant progress has been achieved in bulk crystal growth, epitaxial deposition, defect and impurity control etc. The synthesis of high quality Ga_2O_3 single crystals has been demonstrated. Two inch Ga_2O_3 substrates are already commercially available and larger diameters are being developed. The growth of Ga_2O_3 epitaxial films has been demonstrated by the established state-of-the-art semiconductor techniques such as molecular beam epitaxy (MBE) and metal organic chemical vapour deposition (MOCVD/MOVPE). Proof of concept prototypes of Ga_2O_3 transistors and Schottky diodes have been demonstrated. Applied development of gallium oxide as a perspective semiconductor stimulated basic research aimed at understanding of fundamental material properties.

Gallium oxide can form a number of polymorphs among which the monoclinic β-phase is the most stable. It is commonly accepted that β-Ga_2O_3 has a nearly direct band gap of about 4.8 eV. Semi-insulating or highly conductive n-type material can be produced by appropriate choice of growth conditions or by doping. The origin of n-type conductivity remains controversial. Commonly, n-type conductivity in undoped Ga_2O_3 was attributed to oxygen vacancies; however, theoretic models disprove this assumption and link unintentional n-type conductivity to hydrogen or background impurities such as silicon. The effective electron mass is in the about 0.3 times the free electron mass. Typical electron mobility for Ga_2O_3 at room temperature is in the order of 100 $cm^2V^{-1}s^{-1}$. The possibility to achieve p-type conductivity remains rather illusive because of the high activation energy of acceptors and strong localization of holes. This limits semiconductor applications of Ga_2O_3 to unipolar, Schottky and heterojunction devices.

A growing interest in nanotechnology was another driving force for the Ga_2O_3 research. Low-dimensional Ga_2O_3 nanostructures such as nanowires, nanobelts, nanorods, and nanosheets can be relatively easy produced by a variety of techniques. Nanostructures exhibit different, and in many cases, superior physical properties when compared to those for bulk material. Due to large surface to volume ratio, nanostructures have more surface states to interact with the surroundings. Therefore, nanostructures have many potential applications in catalysis and chemical sensing. The abundance of defect gap states in nanostructures increases light absorption and changes luminescence properties which can be beneficial in photochemical and phosphor applications.

Ga_2O_3 can be used as an efficient host material for rare-earth and transition metal based phosphors. Ferromagnetic doping of Ga_2O_3 has been demonstrated, which opens perspectives for Ga_2O_3 applications in spintronic devices.

However, despite the fact that a significant progress has been made, Ga_2O_3 research and development is still far from being mature. As it can be seen from this review, published data on Ga_2O_3 are still incomplete and somewhat controversial. Open issues such as p-type conductivity and realization of full potential of Ga_2O_3 material for device applications have to be addressed.

ACKNOWLEDGEMENT

This work was funded by the Russian Scientific Foundation under the grant N 14-29-0086. This support is gratefully acknowledged.

REFERENCES

[1] L. de Boisbaudran // *Philos. Mag. Ser.* **4** (1875) 414.
[2] R.Roy, V.G.Hill and E.F. Osborn // *J. Amer. Chem. Soc.* **74** (1952) 719.
[3] H.Y.Playford, A.C.Hannon, E.R.Barney and R.I.Walton // *Chem. - A Eur. J.* **19** (2013) 2803.
[4] L.Li, W.Wei and M.Behrens // *Solid State Sci.* **14** (2012) 971.
[5] S.Yoshioka, H.Hayashi, A.Kuwabara, F. Oba, K. Matsunaga and I. Tanaka // *J. Phys. Condens. Matter.* **19** (2007) 346211.

[6] E.Tronc, C. Chanéac and J.P. Jolivet // *J. Solid State Chem*. **139** (1998) 93.
[7] S.-D. Lee, K. Akaiwa and S. Fujita // *Phys. Status Solidi* **10** (2013) 1592.
[8] J. a Kohn, G. Katz and J.D. Broder // *Am. Minerol.* **42** (1956) 398.
[9] S. Geller // *J. Chem. Phys.* **33** (1960) 676.
[10] G.M. Wolten and A. B. Chase // *J. Solid State Chem.* **16** (1976) 377.
[11] S. Geller // J*. Solid State Chem.* **20** (1977) 209.
[12] J. Ahman, G. Svensson and J. Albertsson // *Acta Crystallogr. Sect. C Cryst. Struct. Commun*. **52** (1996) 1336.
[13] E.G. Víllora, K. Shimamura, T. Ujiie and K. Aoki // *Appl. Phys. Lett.* **92** (2008) 2.
[14] Z. Galazka, K. Irmscher, R. Uecker, R. Bertram, M. Pietsch, A. Kwasniewski, M. Naumann, T. Schulz, R. Schewski and D. Klimm // *J. Cryst. Growth.* **404** (2014) 184.
[15] Z. Guo, A. Verma, X. Wu, F. Sun, A. Hickman, T. Masui, A. Kuramata, M.Higashiwaki, D. Jena and T. Luo // *Appl. Phys. Lett* **106** (2014) 111909.
[16] K.Yamaguchi // *Solid State Commun.* **131** (2004) 739.
[17] H. He, R. Orlando, M. Blanco, R. Pandey, E. Amzallag, I. Baraille and M. Rérat // *Phys. Rev. B.* **74** (2006) 195123.
[18] Y.Zhang, J. Yan, G. Zhao and W. Xie // *Phys. B Condens. Matter.* **405** (2010) 3899.
[19] L. Zhang, J. Yan, Y. Zhang, T. Li and X. Ding // *Sci. China Physics, Mech. Astron*. **55** (2012) 19.
[20] H. Peelaers and C.G. Van de Walle // *Phys. Status Solidi (B)* **252** (2015) 828.
[21] J.B. Varley, J.R. Weber, A. Janotti and C.G. Van de Walle // *Appl. Phys. Lett.* **97** (2010) 142106.
[22] C. Janowitz, V. Scherer, M. Mohamed, A. Krapf, H. Dwelk, R. Manzke, Z. Galazka, R. Uecker, K. Irmscher and R. Fornari // *New J. Phys.* **13** (2011) 085014.
[23] Z. Galazka, R. Uecker, K. Irmscher, M. Albrecht, D. Klimm, M. Pietsch, M. Brützam, R. Bertram, S.Ganschow and R. Fornari // *Cryst. Res. Technol*. **45** (2010) 1229.
[24] J. Zhang, B. Li, C. Xia, G. Pei, Q. Deng, Z. Yang, W. Xu, H. Shi, F. Wu and Y. Wu // *J. Phys. Chem. Solids.* **67** (2006) 2448.
[25] N. Ueda, H. Hosono, R. Waseda and H. Kawazoe // *Appl. Phys. Lett.* **71** (1997) 933.
[26] E.G. Víllora, M. Yamaga, T. Inoue, S. Yabasi, Y. Masui, T. Sugawara and T. Fukuda // *Jpn. J. Appl. Phys.* **41** (2002) L622.
[27] O.M. Bordun, I.Y. Kukharskyy, B.O. Bordun and V.B. Lushchanets // *J. Appl. Spectrosc.* **81** (2014) 771.
[28] M. Passlack, E.F. Schubert, W.S. Hobson, M. Hong, N. Moriya, S.N.G. Chu, K. Konstadinidis, J.P. Mannaerts, M.L. Schnoes and G.J. Zydzik // *J. Appl. Phys.* **77** (1995) 686.
[29] I. Bhaumik, R. Bhatt, S. Ganesamoorthy, A. Saxena, A. K. Karnal, P.K. Gupta, A. K.Sinha and S.K. Deb // *Appl. Opt.* **50** (2011) 6006.
[30] T. Harwig, F. Kellendonk and S. Slappendel // *J. Phys. Chem. Solids.* **39** (1978) 675.
[31] G. Blasse and A. Bril // *Solid State Commun.* **7** (1969) iii.
[32] T. Harwig and F. Kellendonk // *J. Solid State Chem*. **24** (1978) 255.
[33] J.B. Varley, A. Janotti, C. Franchini and C.G. Van De Walle // *Phys. Rev. B - Condens. Matter Mater. Phys*. **85** (2012) 2.
[34] T. Onuma, S. Fujioka, T. Yamaguchi, M. Higashiwaki, K. Sasaki, T. Masui and T. Honda // *Appl. Phys. Lett.* **103** (2013) 2013.
[35] P. Marwoto, S. Sugianto and E. Wibowo // *J. Theor. Appl. Phys*. **6** (2012) 17.
[36] T. Minami // *Solid. State. Electron*. **47** (2003) 2237.
[37] S.-J. Chang, Y.-L. Wu, W.-Y. Weng, Y.-H. Lin, W.-K. Hsieh, J.-K. Sheu and C.-L. Hsu // *J. Electrochem. Soc.* **161** (2014) H508.
[38] M. Martin, R. Dronskowski, J. Janek, K.-D.D. Becker, D. Roehrens, J. Brendt, M.W. Lumey, L. Nagarajan, I. Valov and A. Börger // *Prog. Solid State Chem.* **37** (2009) 132.
[39] K. Matsuzaki, H. Hiramatsu, K. Nomura, H. Yanagi, T. Kamiya, M. Hirano and H. Hosono // *Thin Solid Films* **496** (2006) 37.
[40] R. Moos, N. Izu, F. Rettig, S. Reiß, W. Shin and I. Matinfara // *Sensors* **11** (2011) 3439.
[41] Y. Oshima, E.G. Villora and K. Shimamura // *J. Cryst. Growth* **410** (2015) 53.
[42] G. A.Battiston, R. Gerbasi, M. Porchia, R. Bertoncello and F. Caccavale // *Thin Solid Films.* **279** (1996) 115.
[43] T. Kawaharamura, G.T. Dang and M. Furuta // *Jpn. J. Appl. Phys*. **51** (2012) 2.
[44] J. Hao, Z. Lou, I. Renaud and M. Cocivera // *Thin Solid Films* **467** (2004) 182.

[45] Z. Ji J., Du, J. Fan and W. Wang // *Opt. Mater. (Amst)* **28** (2006) 415.
[46] T. Miyata, T. Nakatani and T. Minami // *Thin Solid Films* **373** (2000) 145.
[47] T. Minami, T. Shirai, T. Nakatani and T. Miyata // *Jpn. J. Appl. Phys*. **39** (2000) L524.
[48] V.N. Maslov, V.I. Nikolaev, V.M. Krymov, V.E. Bugrov and A.E. Romanov // *Phys. Solid State.* **57** (2015) 1342.
[49] D.P. Butt, Y. Park and T.N. Taylor // *J. Nucl. Mater.* **264** (1999) 71.
[50] S. Penner, B. Klötzer, B. Jenewein, F. Klauser, X. Liu and E. Bertel // *Thin Solid Films* **516** (2008) 4742.
[51] R. Binions, C.J. Carmalt, I.P. Parkin, K.F.E. Pratt and G. A. Shaw // *Chem. Mater*. **16** (2004) 2489.
[52] T. Matsumoto, M. Aoki, A. Kinoshita and T. Aono // *Jpn. J. Appl. Phys.* **13** (1974) 1578.
[53] W. Mi, C. Luan, Z. Li, C. Zhao, X. Feng and J. Ma // *Opt. Mater. (Amst)* **35** (2013) 2624.
[54] P. Ravadgar, R.H. Horng and T.Y. Wang // *ECS J. Solid State Sci. Technol.* **1** (2012) N58.
[55] D. Gogova, G. Wagner, M. Baldini, M. Schmidbauer, K. Irmscher, R. Schewski, Z. Galazka, M. Albrecht and R. Fornari // *J. Cryst. Growth* **401** (2014) 665.
[56] G. Wagner, M. Baldini, D. Gogova, M. Schmidbauer, R. Schewski, M. Albrecht, Z. Galazka, D. Klimm and R. Fornari // *Phys. Status Solidi* **211** (2014) 27.
[57] D.J. Comstock and J.W. Elam // *Chem. Mater*. **24** (2012) 4011.
[58] D.H. Kim, S.H. Yoo, T. Chung, K. An, H. Yoo and Y. Kim // *Bull. Korean Chem. Soc*. **23** (2002) 225.
[59] L. Mîinea, S. Suh, S.G. Bott, J.-R. Liu, W.-K. Chu and D.M. Hoffman // *J. Mater. Chem.* **9** (1999) 929.
[60] M. Nieminen, L. Niinisto and E. Rauhala // *J. Mater. Chem.* **6** (1996) 27.
[61] S. Basharat, C.J. Carmalt, R. Palgrave, S.A.Barnett, D.A. Tocher and H.O. Davies // *J. Organomet. Chem.* **693** (2008) 1787.
[62] M. Higashiwaki, K. Sasaki, A. Kuramata, T. Masui and S. Yamakoshi // *Appl. Phys. Lett.* **100** (2012) 013504.
[63] T. Oshima, N. Arai, N. Suzuki, S. Ohira and S. Fujita // *Thin Solid Films* **516** (2008) 5768.
[64] K. Sasaki, M. Higashiwaki, A. Kuramata, T. Masui and S. Yamakoshi // *J. Cryst. Growth* **378** (2013) 591.
[65] K. Sasaki, A. Kuramata, T. Masui, E.G. Víllora, K. Shimamura and S. Yamakoshi // *Appl. Phys. Express* **5** (2012) 035502.
[66] E.G. Villora, K. Shimamura, K. Kitamura and K. Aoki // *Appl. Phys. Lett.* **88** (2006) 031105.
[67] H. Okumura, M. Kita, K. Sasaki, A. Kuramata, M. Higashiwaki and J.S. Speck // *Appl. Phys. Express* **7** (2014) 095501.
[68] M. Schieber // *J. Am. Ceram. Soc.* **47** (1964) 537.
[69] A.B. Chase and J.A. Osmer // *J. Amer. Ceram. Soc.* **50** (1967) 326.
[70] G. Garton, S. Smith and B.M. Wanklyn // *J. Cryst. Growth* **13-14** (1972) 588.
[71] Z. Galazka, R. Uecker, K. Irmscher, M. Albrecht, D. Klimm, M. Pietsch, M. Brützam, R. Bertram, S. Ganschow and R. Fornari // *Cryst. Res. Technol*. **45** (2010) 1229.
[72] Y. Tomm, P. Reiche, D. Klimm and T. Fukuda // *J. Cryst. Growth.* **220** (2000) 510.
[73] V.N. Maslov, V.M. Krymov, M.N. Blashenkov, A.A. Golovatenko and V.I. Nikolaev // *Tech. Phys. Lett.* **40** (2014) 303.
[74] Y. Tomm, J.M. Ko, A. Yoshikawa and T. Fukuda // *Sol. Energy Mater. Sol. Cells* **66** (2001) 369.
[75] E.G. Villora, K. Shimamura, Y. Yoshikawa, K. Aoki and N. Ichinose // *J. Cryst. Growth.* **270** (2004) 420.
[76] N. Suzuki, S. Ohira, M. Tanaka, T. Sugawara, K. Nakajima and T. Shishido // *Phys. Status Solidi (C)* **4** (2007) 2310.
[77] N. Ueda, H. Hosono, R. Waseda and H. Kawazoe // *Appl. Phys. Lett.* **70** (1997) 3561.
[78] S. Ohira, N. Suzuki, N. Arai, M. Tanaka, T. Sugawara, K. Nakajima and T. Shishido // *Thin Solid Films* **516** (2008) 5763.
[79] H.A. Dabkowska and A.B Dabkowski, In: *Springer Handbook of Crystal Growth*, ed. by G. Dhanaraj, K. Byrappa, V. Prasad and M. Dudley (Springer, 2010), p.1817.
[80] A.B. Chase // *J. Am. Chem. Soc.* **47** (1964) 470.
[81] M.R. Lorenz, J.F. Woods and R.J. Gambino // *J. Phys. Chem. Solids* **28** (1967) 403.
[82] L. Binet and D. Gourier // *J. Phys. Chem. Solids.* **59** (1998) 1241.
[83] K. Shimamura, E.G. Villora, K. Muramatu, K. Aoki, M. Nakamura, S. Takekawa, N. Ichinose and K. Kitamura // *J. Japanese Assoc. Cryst. Growth*. **33** (2006) 147.

[84] H. Aida, K. Nishiguchi, H. Takeda, N. Aota, K. Sunakawa and Y. Yaguchi // *Jpn. J. Appl. Phys.* **47** (2008) 8506.
[85] http://www.tamura-ss.co.jp/en/release/20131122/pdf/150210.pdf
[86] http://www.tamura-ss.co.jp/en/release/20131122/
[87] E.G. Víllora, S. Arjoca, K. Shimamura, D. Inomata and K. Aoki // *Proc. of SPIE* **8987** (2014) 89871U.
[88] E.G. Víllora, K. Shimamura, Y. Yoshikawa, T. Ujiie and K. Aoki // *Appl. Phys. Lett*. **92** (2008) 202120.
[89] K. Sasaki, M. Higashiwaki, A. Kuramata, T. Masui and S. Yamakoshi // *Appl. Phys. Express* **6** (2013) 6502.
[90] A. Nag and A. Shireen// *Solid State Commun*. **150** (2010) 1679.
[91] X. Feng, Z. Li, W. Mi, Y. Luo and J. Ma // *Mater. Sci. Semicond. Process* **34** (2015) 52.
[92] L.L. Liu, M.K. Li, D.Q. Yu, J. Zhang, H. Zhang, C. Qian and Z. Yang // *Appl. Phys. A*. **98** (2010) 831.
[93] H. Kawazoe, H. Yanagi, K. Ueda and H. Hosono // *MRS Bull.* **25** (2000) 28.
[94] B. Zheng, W. Hua, Y. Yue and Z. Gao// *J. Catal.* **232** (2005) 143.
[95] Y. Hou, L. Wu, X. Wang, Z. Ding, Z. Li and X. Fu // *J. Catal.* **250** (2007) 12.
[96] C.O. Arean, A.L. Bellan, M.P. Mentruit, M.R. Delgado and G.T. Palomino // *Microporous Mesoporous Mater.* **40** (2000) 35.
[97] O. Takayoshi, K. Kaminaga, H. Mashiko, A. Mukai, K. Sasaki, T. Masui, A. Kuramata, S. Yamakoshi and A. Ohtomo // *Jpn. J. Appl. Phys.* **52** (2013) 111102.
[98] N.K. Shrestha, K. Lee, R. Kirchgeorg, R. Hahn and P. Schmuki // *Electrochem. commun*. **35** (2013) 112.
[99] L.C. Tien, W.T. Chen and C.H. Ho // *J. Am. Ceram. Soc.* **94** (2011) 3117.
[100] S.H. Mohamed, M. El-Hagary and S. Althoyaib // *J. Alloys Compd.* **537** (2012) 291.
[101] K. Girija, S. Thirumalairajan, A.K. Patra, D. Mangalaraj, N. Ponpandian and C. Viswanathan // *Curr. Appl. Phys*. **13** (2013) 652.
[102] K. Girija, S. Thirumalairajan, V.R. Mastelaro and D. Mangalaraj // *J. Mater. Chem. A*. **3** (2015) 2617.
[103] X. Li, X. Zhen, S. Meng, J. Xian, Y. Shao, X. Fu and D. Li // *Env. Sci Technol.* **47** (2013) 9911.
[104] J.H. Kim and K.H. Yoon // *J. Korean Phys. Soc*. **53** (2008) 818.
[105] D. Stodilka, A.H. Kitai, Z. Huang and K.Cook // *SID'00 Digest* (2000) 11.
[106] P. Wellenius, A. Suresh and J.F. Muth // *Appl. Phys. Lett.* **92** (2008) 1.
[107] T. Miyata, T. Nakatani and T. Minami // *J. Lumin.* **87** (2000) 1183.
[108] J.F. Wager, J.C. Hitt, B.A. Baukol, J.P. Bender and D.A.Keszler // *J. Lumin.* **97** (2002) 68.
[109] Y. Tokida and S. Adachi // *ECS J. Solid State Sci. Technol*. **3** (2014) R100.
[110] J.S. Kim, H.E. Kim, H.L. Park and G.C. Kim // *Solid State Commun.* **132** (2004) 459.
[111] P. Wellenius, A. Suresh, J. V. Foreman, H.O. Everitt and J.F. Muth // *Mater. Sci. Eng. B Solid-State Mater. Adv. Technol.* **146** (2008) 252.
[112] P. Patil, J. Park, S.Y. Lee, J. Park and S. Cho // *Appl. Sci. Conv. Technol.* **23** (2014) 296.
[113] G. Sinha and A. Patra // *Chem. Phys. Lett.* **473** (2009) 151.
[114] M. Fleischer, L. Hollbauer, E. Born and H. Meixner // *Am. Cerain.Soc.* **80** (1997) 2121.
[115] M. Fleischer, J. Giber and H. Meixner // *Appl. Phys. A.* **54** (1992) 560.
[116] A. Trinchi, W. Wlodarski and Y.X. Li // *Sensors Actuators, B Chem.* **100** (2004) 94.
[117] S. Nakagomi, K. Yokoyama and Y. Kokubun // *J. Sensors Sens. Syst.* **3** (2014) 231.
[118] S.P. Arnold, S.M. Prokes, F.K. Perkins and M.E. Zaghloul // *Appl. Phys. Lett.* **95** (2009) 103102.
[119] M. Fleischer // *Meas. Sci. Technol.* **19** (2008) 042001.
[120] J.L. Hudgins, G.S. Simin, E. Santi and M.A. Khan // *IEEE Trans. Power Electron*. **18** (2003) 907.
[121] B.J. Baliga // *J. Appl. Phys.* **53** (1982) 1759.
[122] K. Sasaki, M. Higashiwaki, A. Kuramata, T. Masui and S. Yamakoshi // *IEEE Electron Device Lett*. **34** (2013) 493.
[123] T. Oishi, Y. Koga, K. Harada and M. Kasu // *Appl. Phys. Express.* **8** (2015) 031101.
[124] M.A. Rozhkov, E.S. Kolodeznyi, A.M. Smirnov, V.E. Bougrov and A.E. Romanov // *Mater. Phys. Mech*., No 2, Vol. 24, (2015) 194.
[125] W.S. Hwang, A. Verma, H. Peelaers, V. Protasenko, S. Rouvimov, H. (Grace) Xing, A. Seabaugh, W. Haensch, C. Van de

Walle and Z. Galazka // *Appl. Phys. Lett.* **104** (2014) 203111.
[126] W. Hwang, A. Verma and H. Peelaers // *arXiv Prepr. arXiv* (2013) 1.
[127] K Shimamura., E.G. Víllora, K. Domen, K. Yui, K. Aoki and N. Ichinose // *Jpn. J. Appl. Phys.* **44** (2005) L7.
[128] Z.-L. Xie, R. Zhang, C.-T. Xia, X.-Q.Xiu, P. Han, B. Liu, H. Zhao, R.-L. Jiang, Y. Shi and Y.-D. Zheng // *Chinese Phys. Lett.* **25** (2008) 2185.
[129] S. Ito, K. Takeda, K. Nagata, H. Aoshima, K. Takehara, M. Iwaya, T. Takeuchi, S. Kamiyama, I. Akasaki and H. Amano // *Phys. Status Solidi.* **9** (2012) 519.
[130] E.G. Víllora, K. Shimamura, K. Aoki and K. Kitamura // *Thin Solid Films* **500** (2006) 209.
[131] E.G. Villora, K. Shimamura, K. Kitamura, K. Aoki and T. Ujiie // *Appl. Phys. Lett*. **90** (2007) 234102.
[132] V.I. Nikolaev, A.I. Pechnikov, V.N. Maslov, A.A. Golovatenko, V.M. Krymov, S.I. Stepanov, N.K. Zhumashev, V.E. Bougrov and A.E. Romanov // *Mater. Phys. Mech.* **22** (2015) 59.
[133] K. Kachel, M. Korytov, D. Gogova, Z. Galazka, M. Albrecht, R. Zwierz, D. Siche, S. Golka, A. Kwasniewski and M. Schmidbauer // *CrystEngComm.* **14** (2012) 8536.
[134] H.J. Lee, T.I. Shin and D.H. Yoon // *Surf. Coatings Technol*. **202** (2008) 5497.
[135] M.M. Muhammed, M. Peres, Y. Yamashita, Y. Morishima, S. Sato, N. Franco, K. Lorenz, A. Kuramata and I.S. Roqan // *Appl. Phys. Lett*. **105** (2014) 042112.
[136] M. Marezio and J.P. Remeika // *J. Chem. Phys*. **46** (1967) 1862.
[137] H. He, M.A. Blanco and R. Pandey // *Appl. Phys. Lett*. **88** (2006) 2006.
[138] M. Zinkevich, F.M. Morales, H. Nitsche, M. Ahrens, M. Ruhle and F. Aldinger // *Zeitschrift fuer Met. Res. Adv. Tech*. **95** (2004) 756.
[139] G.E.F. Lundell and J.I. Hoffman // *J. Res. Natl. Bur. Stand*. **15** (1935) 409.
[140] S.-A. Lee, J.-Y. Hwang, J.-P. Kim, S.-Y. Jeong and C.-R. Cho // *Appl. Phys. Lett.* **89** (2006) 182906.
[141] S.J. Schneider and J.L. Waring // *J. Res. Natl. Bur. Stand. Sect. A Phys. Chem.* **67A** (1963) 19.